MICROCOPY RESOLUTION TEST CHART

LEVEL

SATELLITE PARTICLE OBSERVATIONS
AND COINCIDENT AURORAL-E IONIZATION

by

James R. Sharber
Department of Physics and Space Sciences
Florida Institute of Technology
Melbourne, FL 32901

Final Scientific Report on Grant AFOSR 78-3625

Prepared for

The Air Force Office of Scientific Research
AFOSR/NP
Bolling AFB, Bldg. 410
Washington, D.C. 20332

DTIC
ELECTE
MAR 1 7 1980

S

A

October, 1979

FIT

SECURITY CLASSIFICATION OF THIS PAGE (When Data Entered)

REPORT DOCUMENTATION PAGE
READ INSTRUCTIONS BEFORE COMPLETING FORM

1. REPORT NUMBER	2. GOVT ACCESSION NO.	3. RECIPIENT'S CATALOG NUMBER
AFOSR-TR-80-0173		

4. TITLE (and Subtitle)	5. TYPE OF REPORT & PERIOD COVERED
SATELLITE PARTICLE OBSERVATIONS AND COINCIDENT AURORAL-E IONIZATION	Final rept. 1 June 78 — 31 Aug 79
	6. PERFORMING ORG. REPORT NUMBER

7. AUTHOR(s)	8. CONTRACT OR GRANT NUMBER(s)
James R. Sharber	AFOSR78-3625

9. PERFORMING ORGANIZATION NAME AND ADDRESS	10. PROGRAM ELEMENT, PROJECT, TASK AREA & WORK UNIT NUMBERS
Florida Institute of Technology P.O. Box 1150 Melbourne, FL 32901	61102F 2311/A1

11. CONTROLLING OFFICE NAME AND ADDRESS	12. REPORT DATE
AFOSR/NP Bolling AFB, Bldg. 410 Washington, DC 20332	31 Oct 1979
	13. NUMBER OF PAGES
	64

14. MONITORING AGENCY NAME & ADDRESS(If different from Controlling Office)	15. SECURITY CLASS. (of this report)
AFOSR-78-3625	unclassified
	15a. DECLASSIFICATION/DOWNGRADING SCHEDULE

16. DISTRIBUTION STATEMENT (of this Report)

Approved for public release; distribution unlimited.

17. DISTRIBUTION STATEMENT (of the abstract entered in Block 20, if different from Report)

18. SUPPLEMENTARY NOTES

19. KEY WORDS (Continue on reverse side if necessary and identify by block number)

Auroral-E
E-Region
Auroral Particles
Diffuse Aurora

20. ABSTRACT (Continue on reverse side if necessary and identify by block number)

Using data taken during coordinated flights of the AFGL Airborne Ionospheric Observatory and the ISIS-2 Satellite, a comparison has been made between the particle spectrum of the continuous (diffuse) aurora and the properties of the auroral-E region with the following results: Most electron differential number spectra of the diffuse aurora may be represented as Maxwellians with characteristic energy between a few hundred eV to a few keV; this characteristic energy increases with pitch angle to a maximum value of 90°. Over the diffuse aurora, the angular distribution of electron energy flux is isotropic only near the peak-

DD FORM 1473 EDITION OF 1 NOV 65 IS OBSOLETE
411665
Unclassified

20.

of precipitation. At latitudes above and below the peak, the energy flux at the edge of the loss cone may exceed that near the local field line by as much as a factor of two. Integration of individual spectra over the loss cone produces a composite Maxwellian distribution which may be used to estimate the electron energy deposited in the E-region. The procedure underestimates the energy by about 20%. Although the continuous (diffuse) aurora is a relatively stable phenomenon, enhancements in intensity of the incident electrons occur on a time scale of a few seconds. It has not been determined whether these variations represent temporal or spatial changes. Within the energy range 10 eV to 15 keV the electron population accounts for 80 - 90% of the particle energy deposited into the E-region. In this energy range the proton population thus accounts for only 10 - 20% of the deposited energy. Sounder measurement of virtual height and critical frequency provides quantitative measures of the electron spectral characteristic energy and total energy flux, respectively. The cause of auroral-E ionization and the diffuse aurora is electron and proton precipitation from the central plasma sheet.

SATELLITE PARTICLE OBSERVATIONS
AND COINCIDENT AURORAL-E IONIZATION

by

James R. Sharber

Department of Physics and Space Sciences

Florida Institute of Technology

Melbourne, FL 32901

Accession For	
NTIS GRA&I	☑
DDC TAB	☐
Unannounced	☐
Justification	
By	
Distribution/	
Availability Codes	
Dist	Avail and/or special
/4	

October, 1979

Approved for Public Release; distribution unlimited

41 665

ABSTRACT

Using data taken during coordinated flights of the AFGL Airborne Iono-
spheric Observatory and the ISIS-2 Satellite, a comparison has been made
between the particle spectrum of the continuous (diffuse) aurora and the
properties of the auroral-E region with the following results: Most elec-
tron differential number spectra of the diffuse aurora may be represented
as Maxwellians with characteristic energy between a few hundred eV to a few
keV; this characteristic energy increases with pitch angle to a maximum
value of 90°. Over the diffuse aurora, the angular distribution of elec-
tron energy flux is isotropic only near the peak of precipitation. At
latitudes above and below the peak, the energy flux at the edge of the loss
cone may exceed that near the local field line by as much as a factor of
two. Integration of individual spectra over the loss cone produces a com-
posite Maxwellian distribution which may be used to estimate the electron
energy deposited in the E-region with an underestimation of the energy by
about 20%. Although the continuous (diffuse) aurora is a relatively stable
phenomenon, enhancements in intensity of the incident electrons occur on a
time scale of a few seconds. Within the energy range 10 eV to 15 keV the
electron population accounts for about 90% of the particle energy deposited
into the E-region. In this energy range the proton population thus accounts
for only about 10% of the deposited energy. Sounder measurements of virtual
height and critical frequency provide quantitative measures of the electron
spectral characteristic energy and total energy flux, respectively. The
cause of auroral-E ionization and the diffuse aurora is electron and proton
precipitation from the central plasma sheet.

TABLE OF CONTENTS

1. INTRODUCTION

The continuous, or diffuse, aurora has become an object of increasing study primarily because of its relative stability and because it represents a major fraction of all particle energy deposited into the auroral iono-sphere. Associated with this diffuse, often subvisual aurora is a relatively thick band of E-region ionization known as auroral-E, apparently caused by the same particles which produce the diffuse aurora (Whalen et al., 1971; Whalen et al., 1977; and Weber et al., 1977). In spite of the fact that a clear association between the diffuse aurora and auroral-E ionization has been made, a detailed investigation of the properties of the incident particle spectrum, and its relation to the properties of auroral-E as measured by an ionosphere sounder, has not been previously undertaken.

The present report which represents such an investigation is the Final Report on Minigrant AFOSR78-3625, "Analysis of Satellite Particle Observations and Coincident Auroral-E Ionization". It results from an analysis of geo-physical data taken as the ISIS-2 polar orbiting satellite made passes over flight paths of the AFGL Airborne Observatory.

Sections 2 - 5 of this report use data taken on the 09 December 1971 flight to investigate the relationship between the spectral parameters of the incident particles and properties of the E-region ionosphere. Section 6 reports the results of a flight over Alaska on 11 December 1971 which is used to study the morphological relationship between the diffuse auroral region and auroral-E. In section 7 the observations are related to the plasma sheet.

The particle measurements were made by soft particle spectrometers aboard ISIS-2, a polar satellite orbiting at 1,400 km. The spectrometers are divergent-plate, electrostatic analyzers; a description of their opera-tion and characteristics is provided in Appendix A.

2. ELECTRON PRECIPITATION OVER THE
CONTINUOUS (DIFFUSE) AURORA

In studying the details of the electron energy spectrum an ISIS-2 satellite pass which occurred during the quiet time between two substorms on 09 December 1971 has been selected. On this day the AFGL Airborne Ionospheric Observatory flew within a constant magnetic local midnight sector while several passes of the ISIS-2 satellite crossed the aircraft path. A number of scientific results of the study have been published (Whalen et al., 1977; Weber et al., 1977; Pike et al., 1977; and Winningham et al., 1978), so the geophysical events of the day are well documented. In Figure 1 (taken from Whalen et al., 1977) the aircraft trajectory is shown as the heavy line plotted in CG latitude and CG longitude coordinates. The ISIS-2 passes are shown as dotted lines, and each is labeled by the universal time at which it crossed the aircraft flight path. For this section emphasis is placed on the particle measurements made by ISIS-2 during the pass labeled 0610. However, it is to be noted for later comparisons that during the leg of the aircraft flight which intersected with the 0610 UT ISIS-2 pass, the CG latitude decreased from about 75° at 0517 UT to about 67° at 0700 UT.

The ISIS-2 electrons for the complete pass over the continuous auroral region are shown in the form of the energy-time spectrogram of Figure 2a. In this presentation each vertical line in the top portion of the graphs represents a differential energy spectrum (ergs/cm^2 ster sec). Intensity is displayed by gray-scale shading with high intensities represented as lighter shades of gray. The logarithm of energy is the ordinate and universal time,

magnetic local time, and invariant latitude are the abscissas. Also shown
in the two graphs in the lower panels are the number and energy fluxes ob-
tained by integration over the energy range of each spectrum. Electron
spectra show very little structure between invariant latitudes of 73° and
66°. This is characteristic of the continuous aurora (Meng, 1976; Deehr
et al., 1976; Lui et al., 1977) and is confirmed in this case by the lack
of any discrete arcs observed at this time by the airborne all-sky camera
(Whalen et al., 1977). Electrons were observed as far poleward as 78.3°;
however these more poleward electrons have a much more sporatic nature and
appear much more structured on the spectrogram.

As shown in Figure 2b, protons were observed between latitudes of
78.5° and 66°. Within the energy range 10 eV to 15 keV, the energy carried
by the protons is low, ≃ 10% of that for the electrons. The proton average
energy increases with decreasing latitude down to about 68° where the broad
spectral peak occurs at an energy of about 10 keV.

Angular Distribution of Energies

ISIS-2 spins at a nominal rate of 22.5 s; thus the electron detectors
which view radially outward scan a range of pitch angles. The effect of
the spin is apparent in Figure 2 where marked decreases in flux occur as
the detector looks downward. The pitch angle is shown in a graph located
just below the energy-time spectrogram portion of the figure. The numbers
above the spectrogram refer to spin cycles of the detector; a cycle is
taken to represent one complete rotation of the satellite.

It is clear from observation of the spin cycles that the electrons are
not always isotropic. In fact spin cycle 4 near the peak of precipitation
is the only cycle which shows isotropy at all energies above about 10 eV.
Cycles 3, 5, 6, and 7 show bites out of the tops of the spin cycles indica-

ting a significant decrease in number and energy flux in the population

nearest the field line. Although a number of workers (for example,

Hultqvist et al., 1974; Winningham et al., 1975) have reported isotropy or

"near isotropy" in the precipitated electron flux over auroras, the fact

that this is not always the case has particular significance with regard

to the effects on the ionosphere.

A clear example of departure from isotropy within the loss cone is

shown in Figure 3. The figure actually shows two pitch angle distributions

made during Cycle 5, labeled as scan 5-1 and scan 5-2. During scan 5-2 the

energy flux near the edge of the loss cone exceeds that near 10° by about a

factor of two. Thus a particle detector viewing directly up the magnetic

field line would in this instance underestimate the precipitated energy by

at least a factor of two if isotropy over the loss cone were assumed.

Electron Energy Spectrum

Figure 4 shows two spectra measured by ISIS-2 during Cycle 5. The

spectrum measured at the largest pitch angle of 37.7° has a prominant Max-

wellian peak and is well represented by the Maxwellian distribution at ener-

gies greater than $\simeq 600$ eV. The spectrum measured at 9.1° shows a Maxwellian

character, but the peak is less prominant and occurs at lower energy. This

spectrum is not as accurately represented by the Maxwellian distribution.

In both spectra, the low-energy portion can be represented with a power

law. This feature occurs with rare exception over auroral latitudes.

The two example spectra from cycle 5 illustrate the general observation

that the electron energy spectrum associated with diffuse aurora can gener-

ally be characterized as Maxwellian in the energy range from a few hundred

eV to about 10 keV. Such a distribution may be written as

$$J(E) = \frac{J_o e}{\alpha} E e^{-E/\alpha} .$$

In this form α is the characteristic energy and J_o is the intensity at the spectral peak (where $E = \alpha$).

As has just been shown in the examples of Figure 4, the energy range over which the spectrum may be reliably represented by a Maxwellian distribution varies with pitch angle. In general the characteristic energy increases with increasing pitch angle reaching a maximum value at a pitch angle of 90°. Another variation in the characteristic energy of the Maxwellian distribution occurs as a function of latitude (or distance across the diffuse auroral form). Both variations bear directly on the energy reaching the E-region, and both will be treated in sections which follow.

3. THE DOWNCOMING DISTRIBUTION
OF ELECTRON ENERGIES

Integration over the Loss Cone

One of the prime objectives of this study is to establish the correspondence between the total energy of precipitated electrons and the critical frequency measured by a bottom side sounder. Thus an accurate determination of electron energy reaching the ionospheric E-region is imperative. Since the downcoming electron energy is, in general, not isotropic, the energy fluxes measured by ISIS-2 must be numerically integrated.

During one complete spin cycle ISIS-2 makes nominally six complete spectral measurements within the loss cone. The total energies Q_i of each spectrum are thus summed according to the following scheme:

$$Q = 0.876 \sum_i Q_i(\theta_i, \theta_z) \cos \theta_i \sqrt{\sin^2 \theta_z - \cos^2 \theta_i} \qquad (3.1)$$
$$\text{(loss cone)}$$

where θ_i represents the pitch angle, θ_z is the angle between the satellite spin axis and the local magnetic field line, and where the sum is performed only over pitch angles within the loss cone. The spectral total energies are thus summed with a weighting function $f(\theta_i, \theta_z)$ as

$$Q = \sum_i Q_i(\theta_i, \theta_z) \, f(\theta_i, \theta_z) \qquad (3.2)$$

where the weighting function

$$f(\theta_i, \theta_z) = (0.876) \cos \theta_i \sqrt{\sin^2 \theta_z - \cos^2 \theta_i} \qquad (3.3)$$

takes into account the detector angular response and the angular spacing and overlap in pitch angle space of successive spectral measurements. The

result Q is then the total electron energy incident on the auroral icnosphere. The function $f(\theta_i, \theta_z)$ is developed in Appendix B.

Maxwellian Distribution of Downcoming Electrons

In order to determine the distribution of electron energies in the downcoming electron beam, equation (3.1) may be applied to individual samples which make up each spectral measurement. In this process, Q_i is replaced by J_i, the differential number flux within each sample, and the result becomes the differential number flux contribution for a given energy sample. Thus a composite spectrum may be constructed, but it is a spectrum already summed over the loss cone and thus represents the <u>downcoming</u> differential number flux (in elec/cm^2 s eV). The rather remarkable result of this kind of sum is a composite spectrum which is well represented by a Maxwellian distribution and whose characteristic energy α and peak intensity J_o provide a very reliable determination of the total energy entering the E-region.

Such a composite spectrum constructed for Scan 5-2 (of cycle 5) is shown in Figure 5. The points are the ISIS-2 measurements; the uncertainty bars are based solely on the accumulated counts and represent the standard deviation of the Poisson distribution. The curve is a Maxwellian with a characteristic energy α of 690 eV and a peak intensity J_o of 1.8×10^5 elec/ cm^2 s eV. It is to be noted that just as for the individual spectra of Figure 4, the Maxwellian curve fit applies to energies greater than 600 eV. The parameters J_o and α give a total energy under the Maxwellian curve over the range $E > 110$ of 0.746 erg/cm^2 s. The direct measurement by ISIS-2 in which the energies of each channel are summed over the range of energies

$E > 110$ gives 0.872 erg/cm^2 s. The percentage difference between these two values is 16%. Thus it is possible, to within very small error, to represent the downcoming electron total energy after summing over the loss cone with a Maxwellian spectrum.

Figures 6a and 6b show a comparison between the total energy of downcoming electrons measured by ISIS-2 and total energy calculated using J_o's and α's obtained from curve fits similar to that of Figure 5 for each spin cycle over the diffuse aurora. The measured values have been determined two ways. In Figure 6a the measured values have been obtained by first integrating the ISIS-2 data over the loss cone to produce the composite spectrum, then summing over the spectral energy intervals. In Figure 6b the measured values have been obtained by first summing each ISIS-2 spectrum (measured at a given pitch angle) over its complete energy range, then integrating this spectral total energy over the loss cone to obtain the total downcoming energy. The two methods of analysis give nearly the same results for measured energies. From each figure it is clear that using J_o and α underestimates the total energy; the amount of underestimation is only 15% near the peak and about a factor of 2 at 72.5^o. In a sum of energies at all latitudes the underestimate of total energy is only 21%.

4. COMPARISON BETWEEN IONOSPHERIC

AND DIRECT PARTICLE MEASUREMENTS

During the flight of 09 December 1971 ionospheric soundings were made
from the AFGL Flying Observatory once each minute with the Granger Model
3905-1 sounder. Each measurement required 20 s to sweep the frequency through
the range 2 to 8 MHz. Flight records were used to obtain the plasma critical
frequency f_oE and the virtual height h'E of the auroral-E layer (Whalen et al.,
1977). In this section a comparison is made between these ionospheric para-
meters and characteristics of the incident electron spectrum measured by
ISIS-2.

Virtual Height

The virtual height h'E is not the true height of the peak electron den-
sity of the E-layer but lies somewhat below it. Whalen et al., (1971) took
h'E to be an estimate of the height at which the ion production rate was a
maximum. This permitted them to infer the kinetic energy of incident elec-
trons using the Rees (1964) calculation of heights of maximum ion production
rate for monoenergetic electrons of isotropic incidence. In the present
study we use the same approach, but now have available a new set of calcula-
tions taken from Strickland (1979), Roble and Rees (1977), and Jones and Rees
(1973). These calculations are made for a Maxwellian spectrum of electrons
incident isotropically on the upper atmosphere. Graphs of altitude of max-
imum ion production vs. incident characteristic energy are shown in Figures
7 and 8. Shown in Table 1 are the aircraft measurements of virtual height
together with the characteristic energies corresponding to peak production

Table 1. Aircraft Measurements of Virtual Height with Characteristic

Energies Corresponding to Peak Production at this Height.

h'(E) (km)	CG Lat.	$E_p(h'E)$ Monoenergetic[1]	$\alpha(h'E)$ Maxwellian[2]
129	67.65	2.5	840
126	67.7	2.9	960
128	67.75	2.6	840
129	67.85	2.5	840
126	67.9	2.9	960
125	68.0	3.1	1000
124	68.1	3.25	1020
122	68.15	3.7	1180
123	68.2	3.5	1100
123	68.3	3.5	1100
121	68.4	4.1	1220
123	68.6	(3.5)	1100
134	70.85	2.00	740
134	71.0	2.00	740
136	71.4	1.82	700
135	72.0	1.92	720
135	72.1	1.88	720
141	72.2	1.52	610
141	72.38	1.52	610
141	72.4	1.52	610
143	72.42	1.45	600
144	72.5	1.38	570
140	72.6	1.52	620
154	72.8	1.05	460
153	72.9	1.07	465
159	73.6	0.94	410

1 Based on Rees (1964)

2 Based on Strickland (1979), Roble and Rees (1977), Jones and Rees (1973)

at this height for monoenergetic electrons (from Figure 7) and for a Maxwellian distribution of electrons (from Figure 8).

One way to compare the ISIS-2 measurements with the aircraft sounder measurements is to compare the spectral peak energy α of the Maxwellian distribution of electrons with the energy derived from the calculations of ion production maxima of Figures 7 and 8. Figure 9 shows such a comparison. The ISIS-2 data, shown as the line curve, are the spectral peak energies obtained from integration over the loss cone over half spins. The data points represent energies derived from the Rees (1964) calculations and have been shifted downward by a factor of 3.7 and to the right (poleward) by about 0.4 of a degree. (The ISIS-2 data are referenced to invariant latitude which can differ from CG latitude by up to 0.5 degree at auroral latitudes). The actual values of the derived energies and the CG latitudes at which they were measured are provided in Table 1.

The requirement of shifting the energies down by the factor of 3.7 shows that the virtual height lies lower in altitude than the height which corresponds to the characteristic energy of the Maxwellian spectrum. This is expected since the Rees (1964) curves use monoenergetic electron beams. A monoenergetic electron beam of energy α will penetrate deeper than a Maxwellian spectrum of characteristic energy α. However, it should be noted that, allowing for some scatter, the two kinds of measurements produce similar latitudinal profiles. In fact the profiles agree very well when one considers that the aircraft took about $\approx 1\frac{1}{2}$ hours to make the virtual height measurements while ISIS-2 took about 4 minutes to measure the energy spectra (refer to Figure 1).

In Figure 10 the ISIS-2 spectral characteristic energies are graphed with data points which represent the Maxwellian characteristic energy for which the maximum ion production rate occurs at the virtual height measured by the aircraft sounder. These data make use of the curve of Figure 8 made from calculations by Strickland (1979), Roble and Rees (1977), and Jones and Rees (1973). Reference to Table 1 shows that the data points have been shifted downward by a factor of about 1.5. This suggests that the virtual height lies below the altitude of the peak in the ion production rate for an incident Maxwellian spectrum.

For example Table 1 shows that at latitude 68.4° a virtual height of 121 km was measured by the aircraft sounder. This corresponds to a Max-wellian characteristic energy of 1220 eV. The actual characteristic energy determined by the ISIS-2 direct particle measurement from Figure 10 is 870 eV. This energy corresponds to an altitude of peak ion production rate of 128 km. Thus the virtual height (of 121 km) lies 7 km below the production peak for this energy.

The latitude profile of derived energies shown as the data points of Figure 10 agrees well with that of the curve of Maxwellian characteristic energies determined from the ISIS-2 measurements. Thus the sounder measure-ment of virtual height h'E may be used as a quantitative measure of the characteristic energy of the Maxwellian distribution of electrons incident on the top of the atmosphere. The procedure involves two steps:

(1) determine the derived energies from virtual height measurements using the curve of Figure 8 (Maxwellian incident spectrum),

(2) divide the derived energies by 1.5.

The result will be an accurate representation of the characteristic energy α of the incident Maxwellian distribution of electrons. As a measure of the accuracy of the procedure, the average deviation of the virtual height measurements from the line through the spectral measurements is 13%.

Critical Frequency

The plasma critical frequency is associated with the maximum electron density $n_e(max)$ of the E-layer by the well-known relation

$$n_e(max) = 1.24 \times 10^4 (f_o E)^2 \qquad (4.1)$$

The ion recombination rate at E-layer maximum is proportional to $n_e^2(max)$, hence to $(f_o E)^4$. Since equilibrium can be assumed, the rates of ion production and recombination are equal, and $(f_o E)^4$ is proportional to the ion production rate at $n_e(max)$. This ion production rate is proportional to the total energy flux deposited by the precipitating particles. This explanation, originally put forth by Omholt (1955) and further supported by Whalen et al. (1971) and Jones (1974), provides the basis for the present comparison between the ISIS-2 measurement of incoming particle energy and $(f_o E)^4$.

The aircraft sounder measurements of $(f_o E)^4$ are plotted in Figure 11 with the total precipitated electron energy measured by ISIS-2. In overlaying the two sets of data the aircraft data have been shifted to the right by 0.4 degree (as with the virtual height measurements). In adjusting the relative magnitudes of the measurements more emphasis has been given to the data between 67° and 69° latitude because (1) this region contains more total energy, (2) the measurements in this region, particularly along the

equatorward edge of each profile, were made at more nearly the same time, and (3) the assumptions of equilibrium and the dependence of electron recombination on $n_e^2(max)$ which apply below $\simeq$ 150 km may not hold for the low energies along the poleward part of the profile since electrons of these energies will be deposited at much higher altitudes.

Although the peaks of the two sets of data do not occur at exactly the same latitude there is general agreement between the two sets of data. On this overlay the peak values of each curve correspond so that the value of $(f_oE)^4$ of 100 MHz^4 corresponds to an incident electron energy of 1 erg/cm^2 s. This is in very good agreement with previous work (Omholt, 1955; Whalen et al., 1971). As a rough measure of the accuracy of this procedure, the average deviation of the $(f_oE)^4$ points from the lines connecting the ISIS-2 data points is 26 %. Thus in using the sounder to determine the total electron energy incident on the E-region ionosphere, the fourth power of the critical frequency is multiplied by 0.01 erg/cm^2 s MHz^4.

5. SYSTEMATICS OF THE LATITUDINAL
PROFILES - GAUSSIAN SHAPE

An interesting result of the comparison between ionospheric and direct particle measurements is that over a significant latitudinal range, the profile of incident electron energy, and the spectral characteristic energy may be approximated by a Gaussian distribution of the form

$$Q = Q_M e^{-\Lambda^2 2/\sigma^2} \hspace{4cm} 4.2$$

where σ is related to the FWHM as FWHM $= 2\sqrt{2\ln2}\ \sigma$. This shape has been shown by Dr. J. A. Whalen (Whalen and Sharber, 1979) to fit several types of measurements each of which reflects the energy incident on the E-region ionosphere. These include emissions of N_2^+ 4278, VUV emissions, ionospheric measurements, and direct particle measurements. The Gaussian approximations to the ISIS-2 total energy profile and to that of the f_oE^4 profile are shown in Figures 12 and 13 respectively. In each case the Gaussian distribution (the solid curve) is characterized by a 3.2° FWHM. In each figure the data near the peak deviates considerably from the Gaussian. In the ISIS-2 data of Figure 12 the deviation occurs during spin cycle 4 (latitude 69.4°), the only spin cycle for which the downcoming energy was isotropic.

These Gaussian fits are by no means rigorous but they do suggest some regularity in a description of the diffuse aurora. From the ratio of the two curves we obtain a conversion factor between the sounder measurement of f_oE^4 and the downcoming electron energy of 0.0092 erg/cm^2 s MHz^4, which does not differ greatly from the value of 0.01 erg/cm^2 s MHz^4 obtained in the previous section.

The characteristic energies may also be approximated by Gaussian distributions in latitude. In Figure 14 a Gaussian distribution of $3.5°$ FWHM has been fitted to the ISIS-2 characteristic energies (α) of the downcoming Maxwellian spectra calculated for each half spin cycle. The fit is good for points above the half-maximum, but it is clear that the curve deviates from the data at lower values of α.

The Gaussian fit to the Maxwellian characteristic energies which correspond to measured values of virtual height based on calculations by Strickland (1979) (see Table 1 and Figure 10) is shown in Figure 14. The curve is characterized by an FWHM of $3.5°$ as was done in Figure 13 for the ISIS-2 measurements. The points along the equatorward edge and up to a latitude of about $71.5°$ are well represented by the Gaussian. The fact that the points along the poleward portion of the profile may be fitted with a segment of the same Gaussian curve suggests that a spatial or temporal change may have occurred as the aircraft flew toward lower latitudes. However, this can only be regarded as a possibility, since in general, for moderate to active times, the best Gaussian curve fit is consistently the equatorward edge of the latitudinal profile (Whalen and Sharber, 1979).

A comparison of peak values of the Gaussian curve fits of Figures 14 and 15 give a ratio of 1.2 between the characteristic energies of Strickland's calculations and those measured by ISIS-2.

The fact that the spectral characteristic energies (Figures 14 and 15) are fitted by a broader Gaussian than the total energies (Figures 12 and 13) indicates that for this pass the number flux of downcoming electrons near the center of the diffuse auroral form is greater by at least 30% than near the edges.

6. FLIGHT OF 11 DECEMBER 1971

On universal days 10 and 11 December, 1971, the AFGL Airborne Observatory flew over the Alaskan chain of observatories for approximately nine hours. A portion of the flight path is shown plotted in CG latitude/CG local time in Figure 16. During the flight, ISIS-2 made three crossings of the flight path. As the plane flew the southward leg of the flight shown in the figure, the satellite made two passes over the region, one during hour 07 UT (Orbit 3229) and one during 09 UT (Orbit 3230). Although the aircraft sounder measurements and satellite particle measurements were not simultaneous, the two satellite passes bracketed the aircraft path both in universal time and local time. ISIS-2 detected keV-energy electrons at latitudes shown by the shaded rectangles along the orbits. The aircraft sounder detected the auroral-E layer between 0828 and 0853 UT as shown by the cross-hatched region along the path. Also shown in the figure are the measurements of the auroral-E layer by the aircraft early in the flight ($\approx$ 0520 to $\approx$ 0540 UT).

It is apparent from looking at Figure 16 that the presence of keV electrons does not necessarily indicate auroral-E ionization. In general the equatorward boundary locations of about 68° agree but electrons were observed by ISIS-2 to extend much further poleward reaching a latitude of 74.2° on Orbit 3229 and 71.5° on Orbit 3230. It is felt that the reason for this difference is to be found in the characteristics of the particles precipitating into the auroral ionosphere.

The ISIS-2 electrons and protons measured during Orbit 3229 and Orbit 3230 are displayed with the sounder measurements of h'E and foE" in Figure 17.

Also indicated in the figure is the region where $h'E_s$ and foE_s (virtual height and critical frequency for sporadic E) were detected. The three panels of the figure are arranged in order of time of measurement (UT) from top to bottom and have been aligned horizontally in invariant latitude. The following observations are clear from the figure:

1. On Orbit 3229 (0917:05 UT) keV electrons were detected by ISIS-2 between invariant latitudes 68.1° and 74.2°. Protons were observed between latitudes 67.7° and 73.4°.

2. Approximately two hours later during Orbit 3230 (0912:17 UT) ISIS-2 measured keV electrons between 68.1° and 71.5°. Protons were observed between latitudes of 67.8° and 70.5°.

3. The aircraft sounder detected the auroral-E layer between latitudes of 67.8° and 70.2°.

The auroral electron data of both Orbit 3229 and Orbit 3230 show that electron precipitation occurs in two distinct regions. These regions have been designated CPS (central plasma sheet) and BPS (boundary plasma sheet) by Winningham et al. (1975) and by Lui et al. (1977). The BPS is the most poleward of the two regions and is characterized by structure on the energy-time spectrogram suggestive of discrete and auroral arcs. During the pass of Orbit 3229 the BPS region extended from 74° down to approximately 70.5°; during Orbit 3230 the BPS extended from 71.5° down to about 70°. The CPS lies equatorword of the BPS, is most often adjacent to the CPS, and maps directly into the central part of the plasma sheet. The energy-time spectrogram associated with the CPS usually lacks much structure suggesting a broadly peaked spectrum and diffuse aurora. Figure 17 shows that protons

may be found in both the BPS and CPS regions but are prominant in the CPS.
During the pass of Orbit 3229 the CPS was located between latitudes 70.5°
and 67.7°; on Orbit 3230 the CPS was located between about 70° and 67.8°.
Thus it is clear that the auroral-E ionization layer corresponds very closely
with the CPS region of particle precipitation and is therefore generally
caused by the influx of both electrons and protons. This observation makes
clear the association between the auroral-E layer and the plasma sheet.

In light of a recent paper by Bresprozvanaya and Shchuka (1977), which
concludes that auroral-E is caused exclusively by precipitating protons, and
other experimental results (Montalbetti and McEwen, 1962; Mahlem, 1962; and
Eather and Jacka, 1966) which provide clear correlation auroral-E and H_{β}
emissions, it is worth noting that on Orbit 3230 the auroral-E ionization
does correspond closely with the precipitating protons (see Figure 17). On
Orbit 3229 the protons extend somewhat further poleward than the auroral-E
layer; however most of the protons are found within latitudes spanned by
auroral-E. But it must be pointed out here that Figure 17 shows that preci-
pitating electrons were also present at latitudes on which the auroral-E was
observed. These electrons have a Maxwellian spectral shape at E-region
energies and would therefore give rise to a thick layer of E-region ioniza-
tion just as would the protons. Another example already presented in
Figure 6 shows electrons at the same latitudes as protons. This is a general
property of the auroral regions as determined by ISIS-2 SPS observations.
Thus this report leaves no doubt that electrons as well as protons are re-
sponsible for the production of the auroral-E layer.

The question of which particle population deposits the greatest amount of energy into the upper atmosphere cannot be completely answered at this time since the ISIS-2 SPS only measures the particle spectra over the range $\simeq$ 10 eV to $\simeq$ 15 keV. However, within this range of energies, the SPS measurements show that the electrons carry 80 to 90% of the total energy. In both the 0610 UT pass of 09 December 1971 shown in Figure 6 and the 0719 and 0912 UT passes of 11 December 1971 shown in Figure 17, the electron spectra peak around 1 keV while the proton spectra peak at 6 - 10 keV. It is not known, however, whether there is a second peak in either spectrum at an energy greater than 15 keV. Such a peak in the proton spectrum could cause the proton population to be the dominant contributor of energy to the E-region.

7. RELATIONSHIP OF THE OBSERVATIONS

TO THE PLASMA SHEET

The association between the continuous (diffuse) aurora and the auroral-E layer has been made by Whalen et al. (1977) and Weber et al.(1977) in an analysis of coincident aircraft and satellite data taken on 09 December 1971. In the present report it is clearly demonstrated that not only are the precipitating particles responsible for the auroral-E layer, but that this auroral-E layer, associated with the diffuse aurora, is also associated with the earthward extension of the central plasma sheet (CPS). Thus auroral-E ionization results directly from particles precipitating from the plasma sheet, and the properties of this ionization layer are therefore a direct consequence of processes taking place in the plasma sheet itself.

The link between the low-altitude CPS region and the central region of the plasma sheet has already been made by Winningham et al. (1975) and Lui et al. (1977). The paper by Lui et al. cited the general similarity between energy spectra of the plasma sheet and spectral characteristics of the CPS region and the similarity in the softening of the electron spectrum at the inner edge of the plasma sheet (Vasyliunas (1968) and Frank (1971) and at the equatorward edge of the CPS region as seen in the ISIS data.

A recent study by Kivelson, Kaye, and Southwood (1979) has provided strong theoretical support for the similarity in the softening of the particle spectra at the inner edge of the plasma sheet and at the equatorward edge of the low-altitude CPS region. The study explained observations of

magnetospheric plasma as seen from a geosynchronous orbit by modeling the magnetospheric electric and magnetic fields and determining steady state demarcation boundaries (SSDB's) for particles of various energies and magnetic moments. The SSDB's separate drift paths which close upon themselves in the middle magnetosphere from those which are open to the tail lobes and the magnetopause. A set of such boundaries taken from Kivelson, Kaye and Southwood (1979) is shown in Figure 18 for plasma sheet electrons of energies 0, 0.75, 4.5, and 12 keV. The model employed a dipole magnetic field and a uniform, steady state, dawn-dusk electric field of 1 kV/R_E.

The boundaries at local midnight for these energies have been mapped to auroral latitudes using $\cos^2 \Lambda = 1/L$, where L is the equatorial crossing point of the field line. The results are in Figure 19. The shape of the curve is similar to those which show the decrease in electron spectral characteristic energy (Figure 14) and the decrease in electron total precipitated energy (Figure 12) with decreasing latitude. Thus the shape of the latitudinal profile of spectral characteristic energy may be explained by considering drift paths in a steady state model of the magnetosphere.

Another result of the work of Kivelson, Kaye and Southwood (1979) shows that as the magnetospheric electric field increases, the SSDB's at all energies move inward (toward the earth). Thus the latitude below which no electrons are observed (this corresponds to the zero energy point of Figure 18) may be used as a qualitative indicator of the strength of the magnetospheric electric field.

Another possibility of probing the magnetospheric electric field from a low altitude polar orbiting satellite arises from the pitch angle

distribution of characteristic energies observed over the diffuse aurora. Figure 4 illustrates this effect for the 0610 UT pass of 09 December 1971 where it is shown that the characteristic energy of the Maxwellian spectrum increases toward the edge of the loss cone. In fact, the characteristic energy increases to a maximum at 90° and reaches a minimum at 180°. This is illustrated in Figure 20 which plots the results of a Maxwellian curve fit to the highest energy population of each spectrum measured during the pass of 0954 UT of 09 December 1971. In the figure the characteristic energy is plotted against invariant latitude and universal time. The figure shows that during each spin cycle the characteristic energy undergoes a systematic change showing a maximum value at a pitch angle of 90°, a minimum at 180°, and an intermediate value (local minimum) at 0°.

As shown in the study reported by Kivelson et al. (1979), the steady state demarcation boundaries, and in fact the time dependent demarcation boundaries (TDDB's) (Kaye and Kivelson, 1979), are functions of particle energy and pitch angle. Thus the pitch angle distribution of characteristic energies might provide a way of determining the strength of the magneto-spheric electric field. This has not been pursued for the present report, but remains an interesting possibility and is recommended for further study.

8. CONCLUSIONS

The current study has revealed the following:

(1) The Maxwellian character of the electron spectrum at energies above a few hundred eV has been demonstrated.

(2) The characteristic energy of the Maxwellian distribution increases with pitch angle to a maximum value at 90°.

(3) Over the diffuse aurora, the angular distribution of electron energy flux is isotropic only near the peak of precipitation. At latitudes above and below the peak, the energy flux at the edge of the loss cone may exceed that near the local field line by as much as a factor of two.

(4) Integration of individual spectra over the loss cone produces a composite Maxwellian distribution which may be used to estimate the electron energy deposited in the E-region. The procedure underestimates the energy by about 20%.

(5) Although the continuous (diffuse) aurora is a relatively stable phenomenon, enhancements in intensity of the incident electrons occur on a time scale of a few seconds. It has not been determined whether these variations represent temporal or spatial changes.

(6) Sounder measurement of virtual height h'E may be used as a quantitative measure of the characteristic energy of the Maxwellian distribution of electrons incident on the atmosphere. The procedure is to use the ionization rate curve of Figure 8 to derive a characteristic energy for each measured h'E value. This derived characteristic energy is multiplied by 1.5 to determine the characteristic energy of the incident electron spectrum.

(7) The sounder measurement of critical frequency may be used as a quantitative measure of the total electron energy incident on the atmosphere. To obtain this incident energy requires multiplication of $(f_oE)^4$ by 0.01 erg/cm^2 s MHz^4.

(8) The cause of auroral-E ionization and the continuous (diffuse) aurora is electron and proton precipitation from the low-altitude extension of the central plasma sheet (CPS) region.

(9) Within the energy range 10 eV to 15 keV the electron population accounts for 80 - 90% of the particle energy deposited into the E-region. In this energy range the proton population thus accounts for only 10 - 20% of the deposited energy.

9. FIGURE CAPTIONS AND FIGURES

Fig. 1: CG latitude and longitude plot of aircraft trajectory (heavy line) of 09 December 1971. The ISIS-2 passes are shown as dotted lines and are labeled by the universal time of crossing the aircraft flight path. The 0610 pass and 0954 pass are used in the present study.

Fig. 2: ISIS-2 electron and proton spectrograms for the 0610 UT of 09 December 1971 shown in Figure 1. Spin cycles referred to in the text are labeled at the top of the figure.

Fig. 3: Angular distribution of electron energies measured by ISIS-2 during Cycle 5 (0610:36 UT - 0610:57 UT) of the pass of 09 December 1971 shown in Figure 2. The loss cone is 49.5° at the satellite altitude of 1400 km.

Fig. 4: Electron differential number spectra measured within the loss cone during Cycle 5. The spectrum measured at a pitch angle of 37.7° carries almost twice as much energy as that measured at 9.12°.

Fig. 5: Differential number spectrum of electrons summed over the loss cone during scan 5-2. The smooth curve is a Maxwellian of the form $J(E) = (J_o e/\alpha) E\, e^{-E/\alpha}$ with $\alpha = 690$ eV and $J_o = 1.8 \times 10^5$/cm s eV. These parameters accurately represent the energy reaching the E-region.

Fig. 6: Comparison between total energy flux of downcoming electrons measured by ISIS-2 and total energy flux calculated using Maxwellian parameters J_o and α obtained from curve fits of composite spectra for each spin cycle over the diffuse aurora. In (a) the measured values were obtained by first integrating over the loss cone

then summing over energy intervals. In (b) the measured values were obtained by first summing each spectrum over its complete energy range, then integrating this total energy flux over the loss cone.

Fig. 7: Altitude of peak ion production rate for monoenergetic electrons (Rees, 1964) and protons (Eather and Burrows, 1967) at isotropic incidence.

Fig. 8: Altitude of peak ion production rate for electrons of Maxwellian spectrum of characteristic energy α at isotropic incidence. The points for the curve are taken from calculations of Strickland (1979), Roble and Rees (1977) and Jones and Rees, 1974.

Fig. 9: Comparison between characteristic energy α of incident electrons (line curve) and E (h'E) from Rees (1964) (points). The points have been shifted downward by a factor of 3.7. See Table 1 for actual values.

Fig. 10: Comparison between Maxwellian characteristic energy α of incident electrons (line curve) and characteristic energy α (h'E) derived from Figure 8 (points). The points have been shifted downward by a factor of 1.5. See Table 1 for actual values.

Fig. 11: Comparison between latitudinal profiles of the ISIS-2 measurement of downcoming energy flux (crosses) and the aircraft sounder measurement of $(f_oE)^4$ (circles).

Fig. 12: ISIS-2 measurements of downcoming energy flux (crosses) fitted with a Gaussian of 3.2^O FWHM (curve).

Fig. 13: Aircraft sounder measurements of $(f_oE)^4$ (circles) fitted with a Gaussian of 3.2^O FWHM (curve).

Fig. 14: ISIS-2 measurements of spectral characteristic energy (circles) fitted with a Gaussian of 3.5° FWHM.

Fig. 15: Aircraft sounder determination of characteristic energy (circles) fitted with a Gaussian of 3.5° FWHM.

Fig. 16: Aircraft and satellite trajectories over Alaska on 11 December 1971 plotted in CG latitude and CG local time. During the satellite passes, identified by orbit numbers 3228, 3229, and 3230, keV electrons were measured at latitudes indicated by shading. During the aircraft flight, the auroral-E layer was measured at latitudes indicated by cross hatching. The small numbers along each trajectory are universal time markers.

Fig. 17: Spectrograms of ISIS-2 electrons and protons measured during orbits 3229 and 3230 plotted on a common invariant latitude scale with aircraft sounder measurements of virtual height h'E and critical frequency $(f_oE)^4$ (also see Figure 16). The auroral-E layer corresponds to the low-altitude extension of the central plasma sheet (CPS) region.

Fig. 18: Steady state demarcation boundaries (SSDB's) for quiet times for energies 0, 0.75, 4.5, and 12 keV computed by Kivelson et al. (1979) using a uniform dipole magnetic field and a uniform cross-tail electric field of strength 1 kV/R_E.

Fig. 19: SSDB boundaries of Figure 18 mapped to auroral latitudes using $\cos^2\Lambda = 1/L$. The dashed line marks the latitude boundary for 0 keV.

Fig. 20: Spectral characteristic energy vs. latitude measured during the
ISIS-2 pass of 0954-0956 UT of 09 December 1971. The figure shows
that during each spin cycle (see pitch angle information at top)
the characteristic energy undergoes a systematic change with a
maximum value at 90°, a minimum at 180°, and an intermediate value
(local minimum) at 0°.
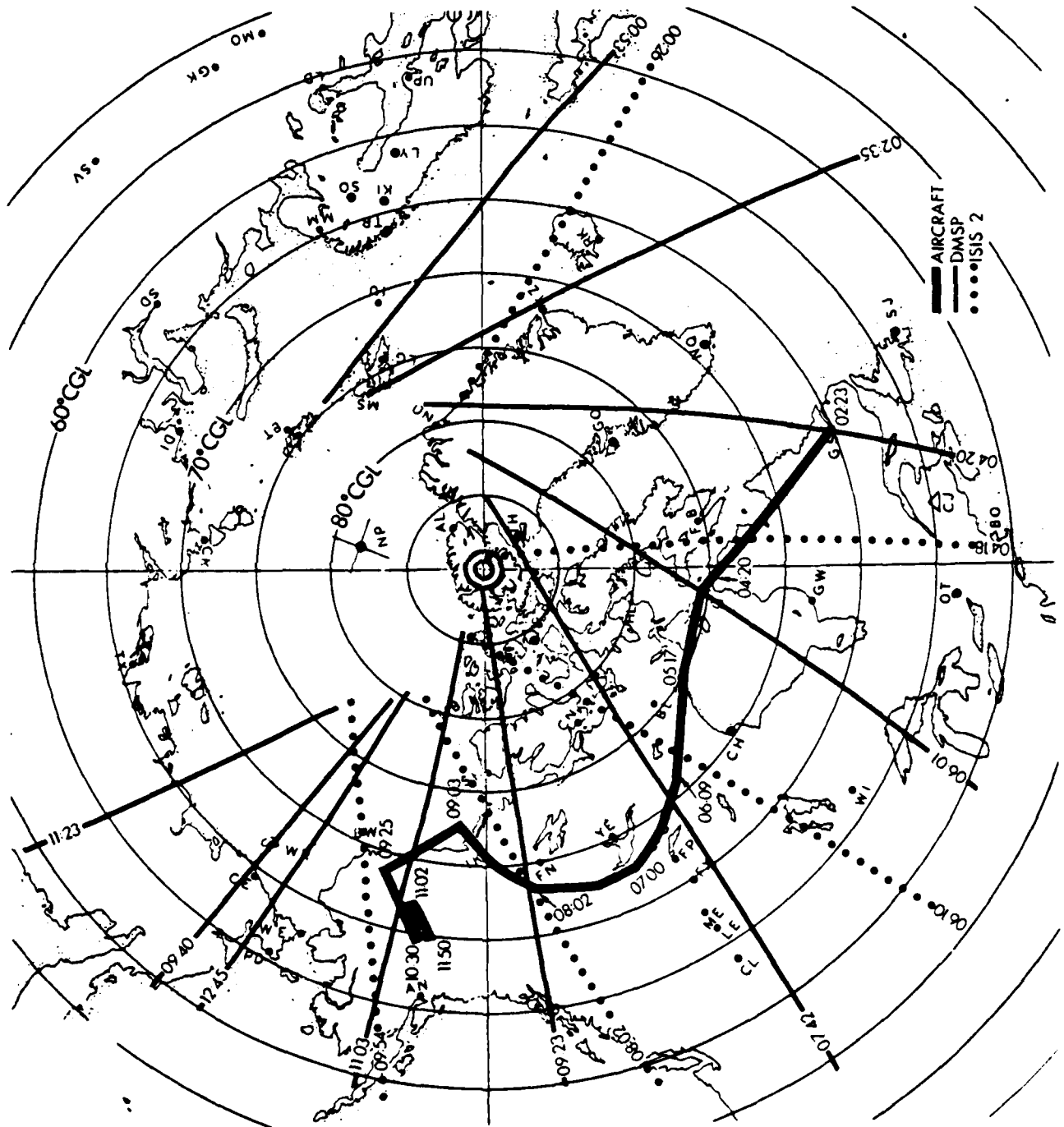
Figure 1

Figure 2

Figure 3

θ = 37.7°
0610:48 UT
E = 0.48 erg/cm²s sr eV
J_o = 1.5 x 10⁵/cm²s sr eV
∝ = 940 eV

θ = 9.12°
0610 46 UT
E = 0.27 erg/cm²s sr eV
J_o = 10⁵/cm²s sr eV
∝ = 800 eV

J (elec/cm²s eV sr)

ENERGY   (eV)
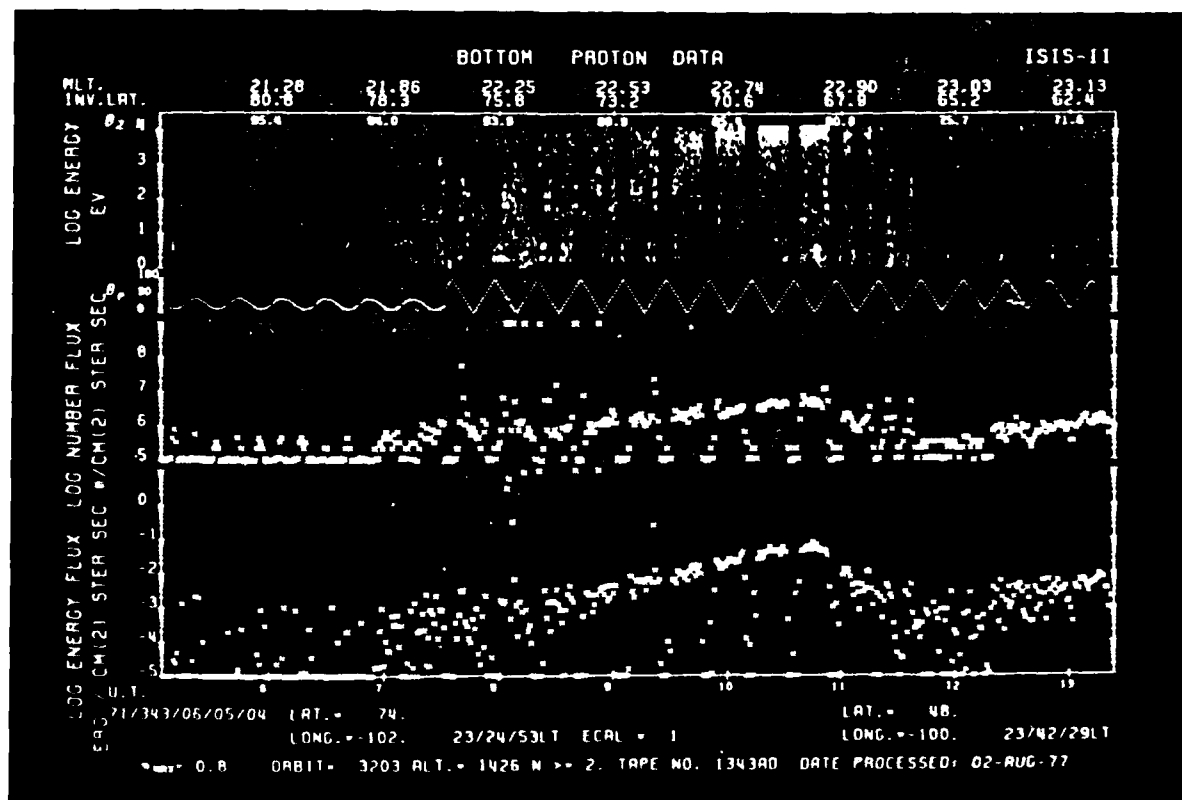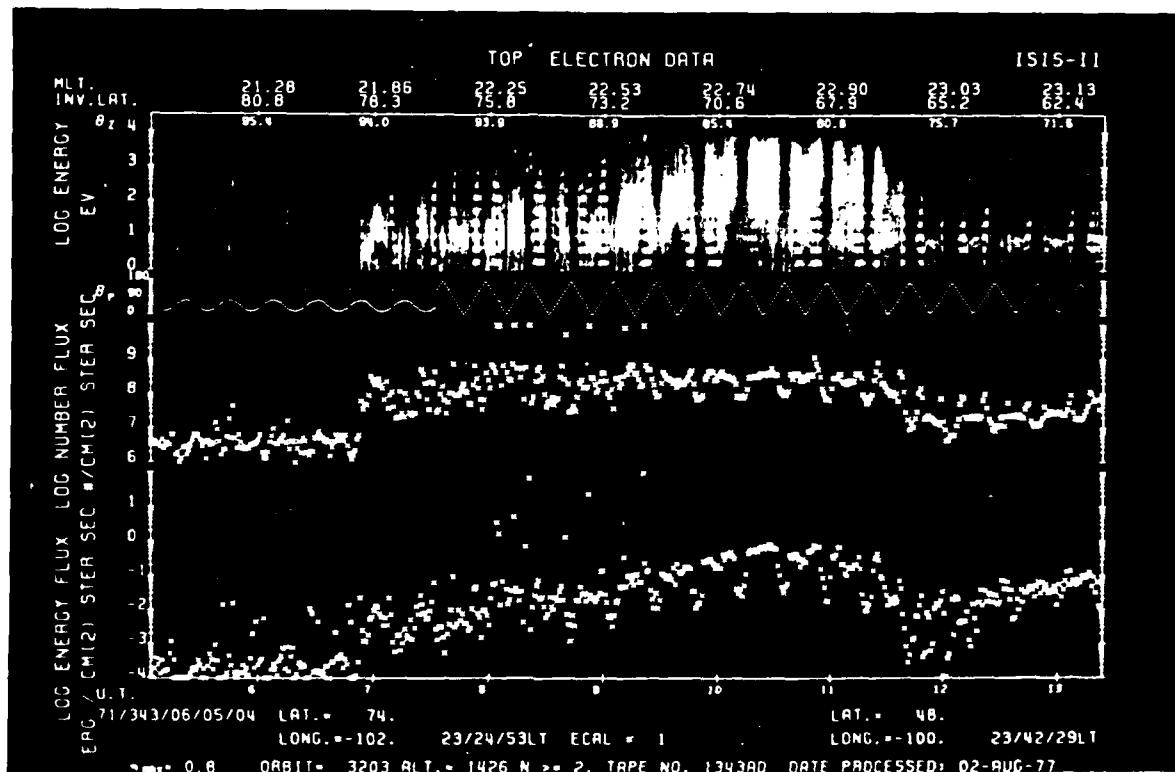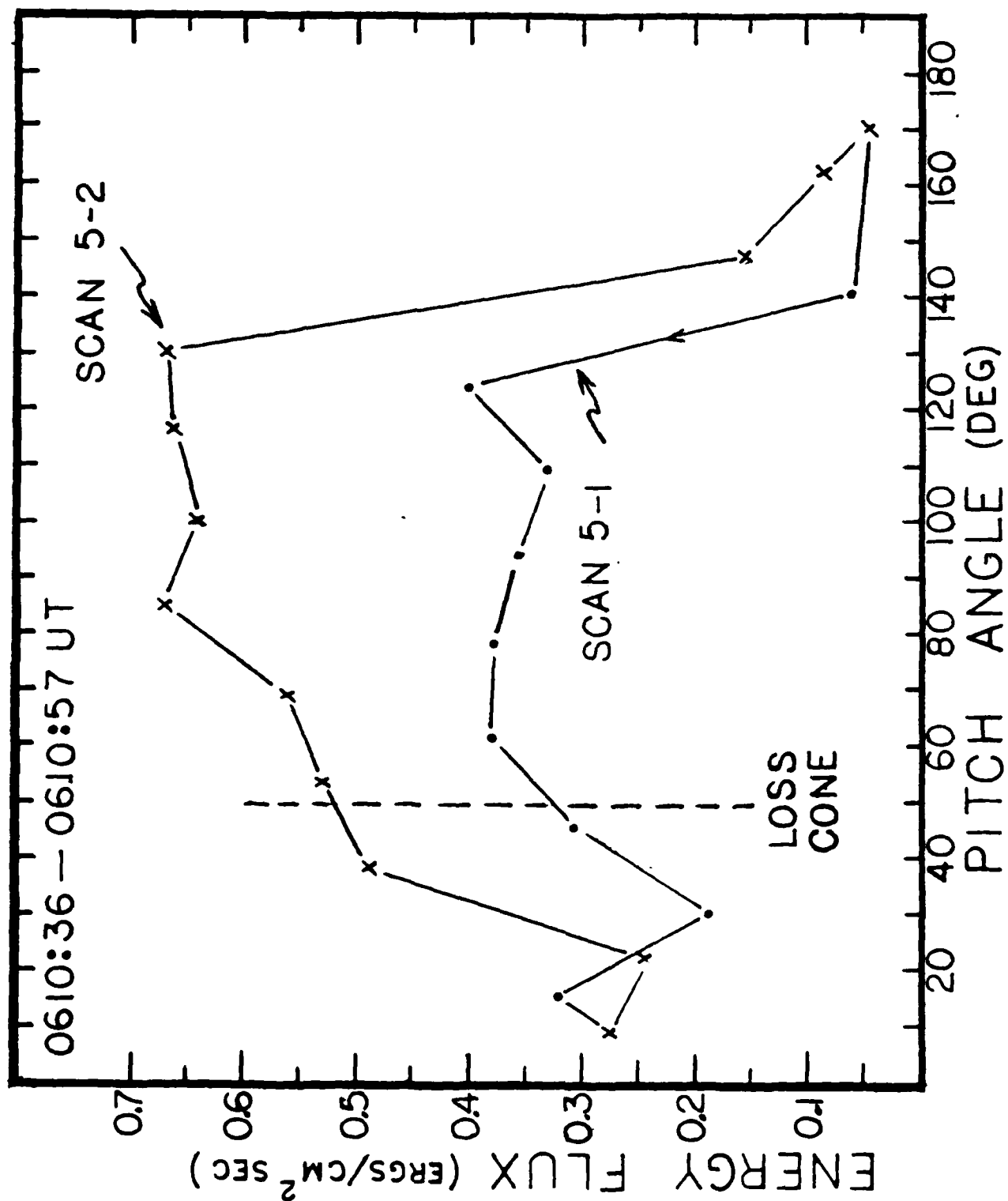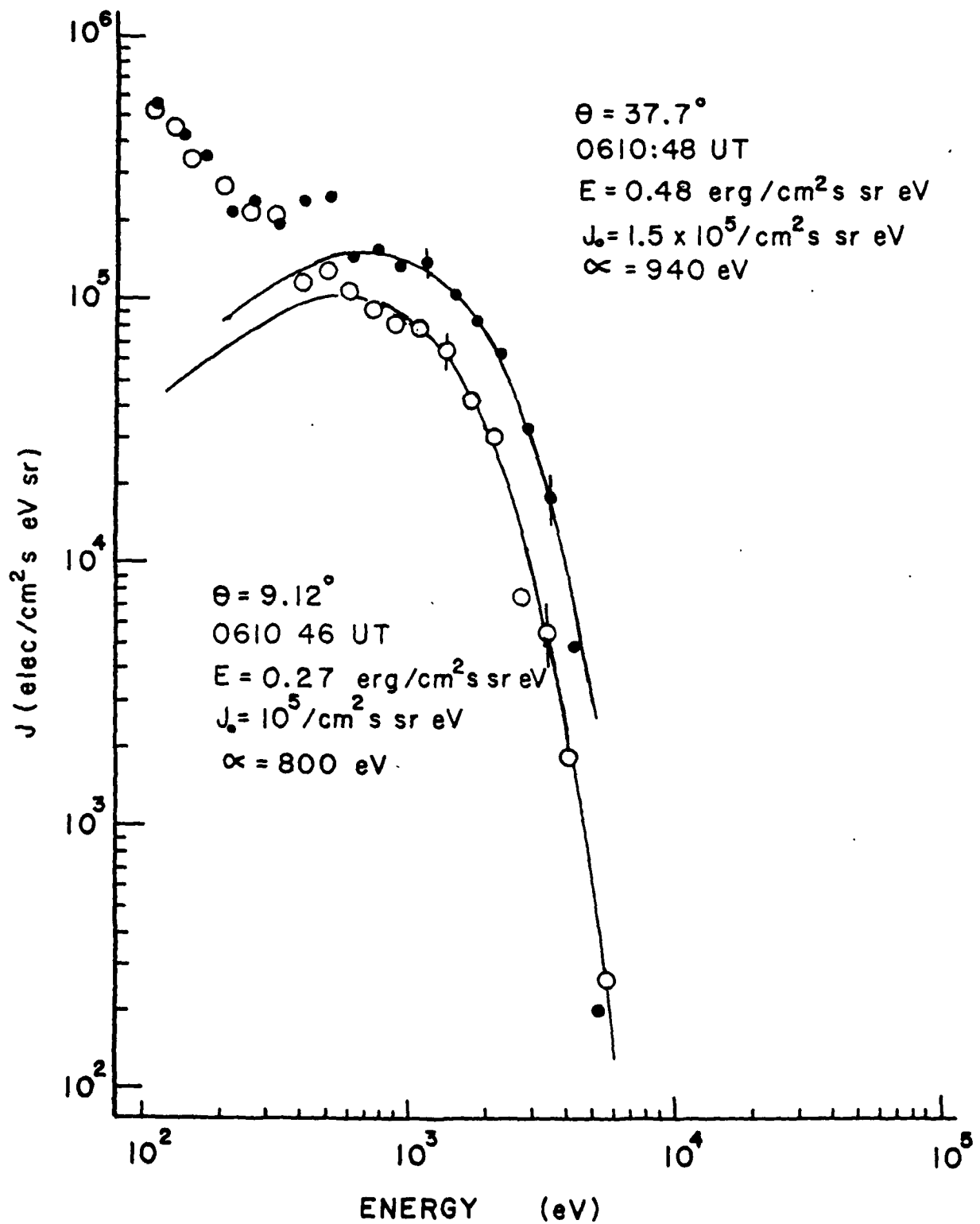
Figure 4

COMPOSITE MAXWELLIAN

SCAN 5-2

$\alpha = 690$ eV

$J_0 = 1.8 \times 10^5 / cm^2 \, s \, eV$

Y-axis: DIFFERENTIAL NUMBER FLUX (elec/cm^2 s eV)

X-axis: ENERGY (eV)
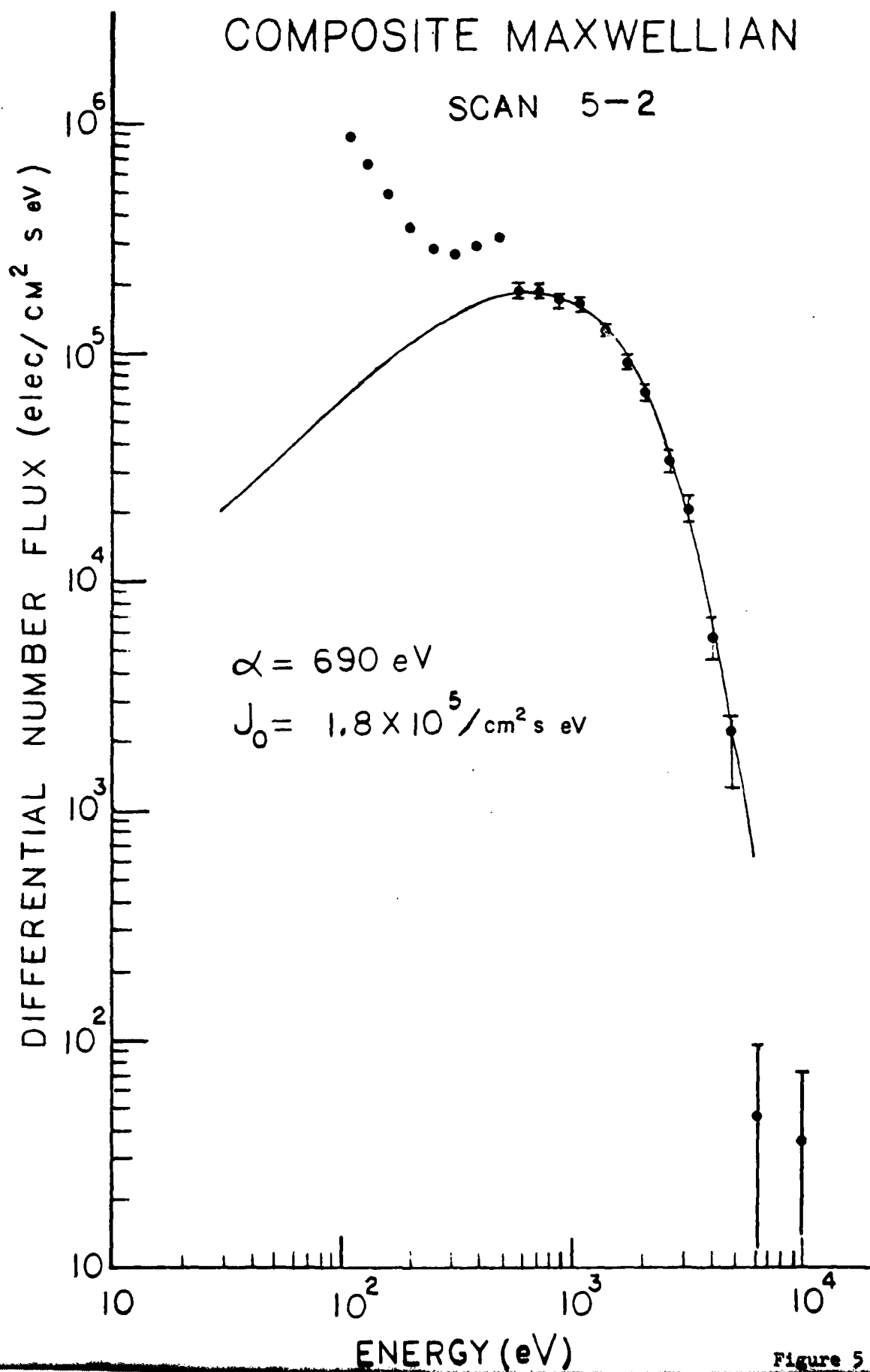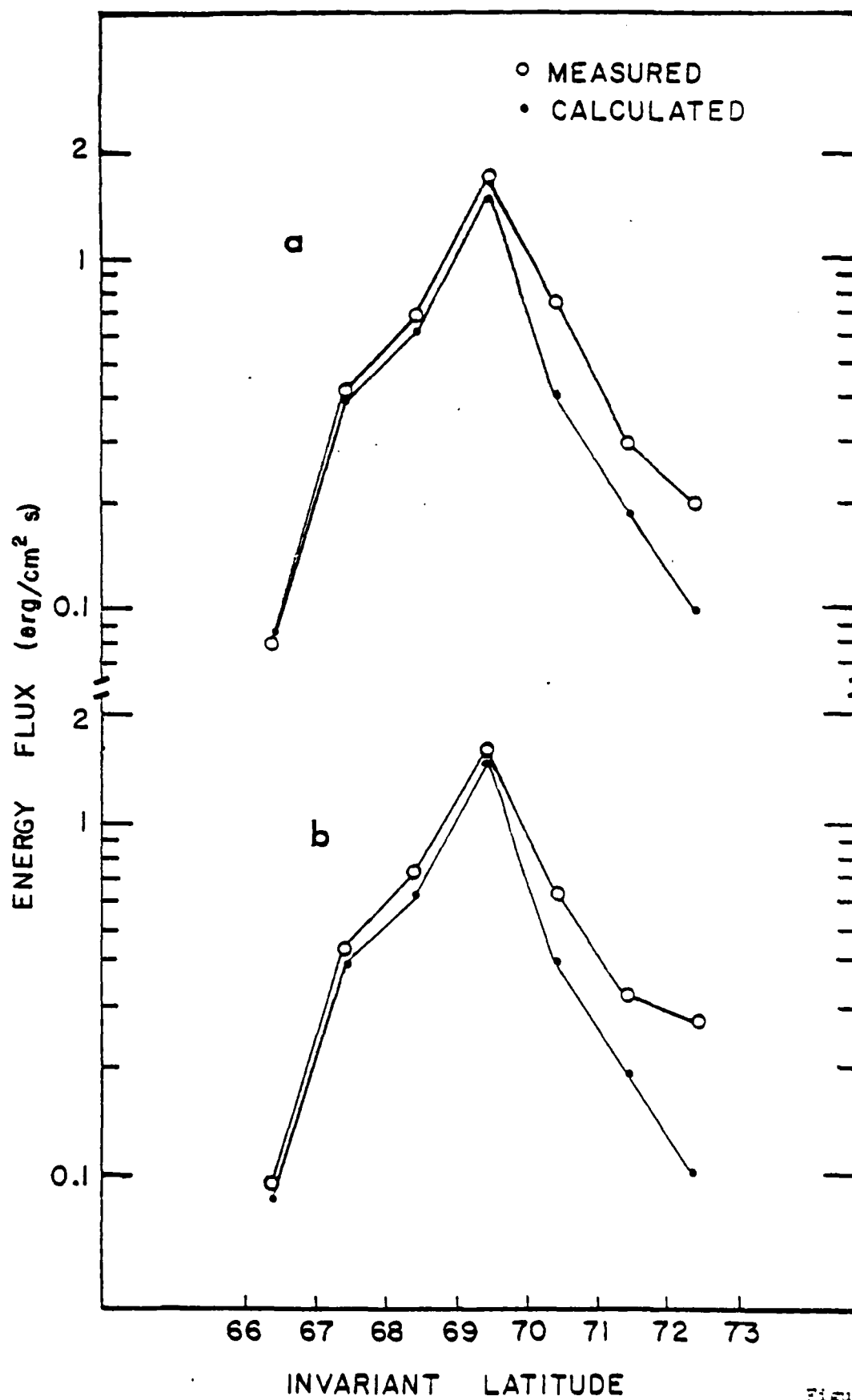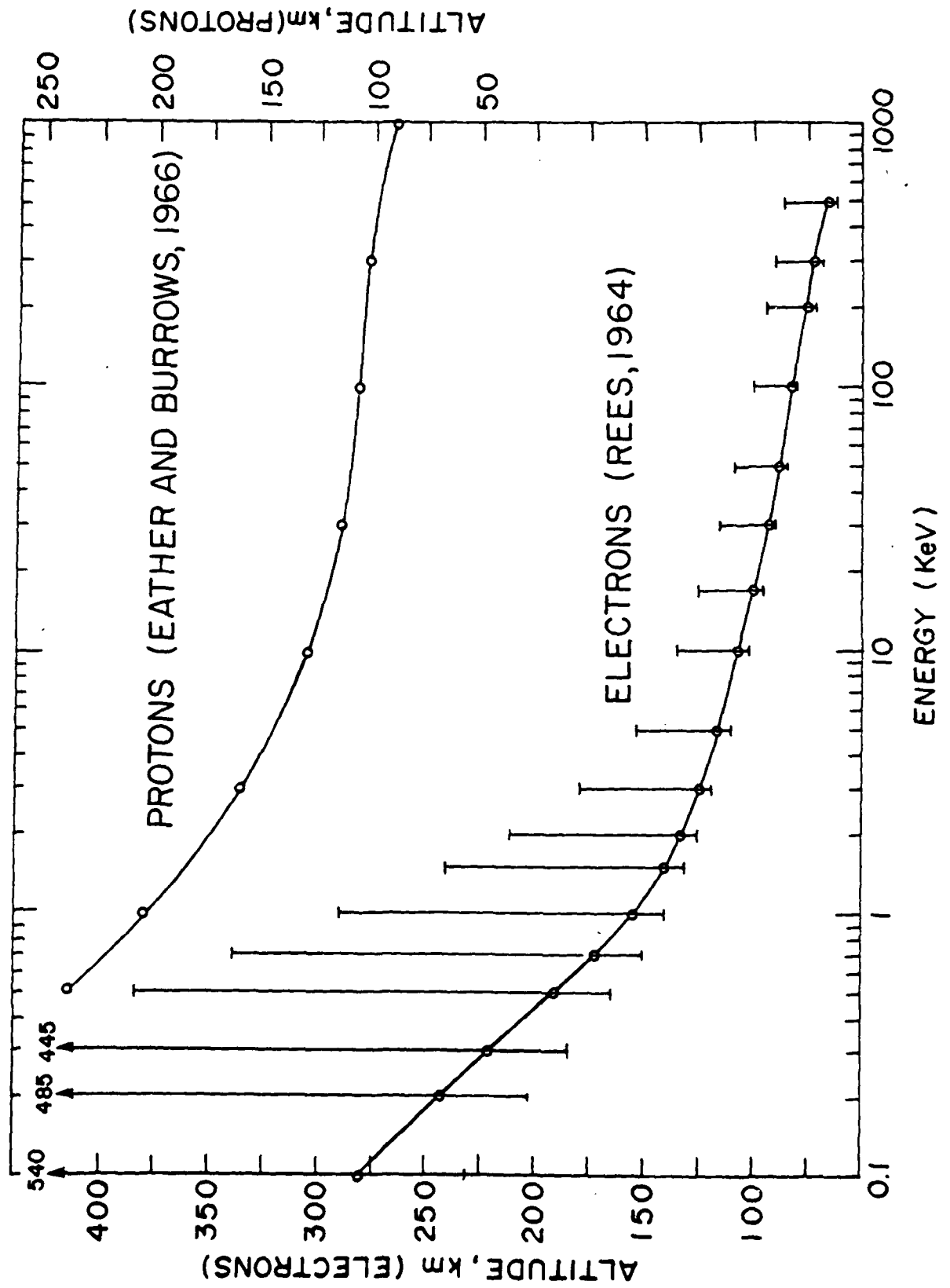
Figure 5

Figure 6

Figure 7

Figure 8

Figure 9

ENERGY (eV)
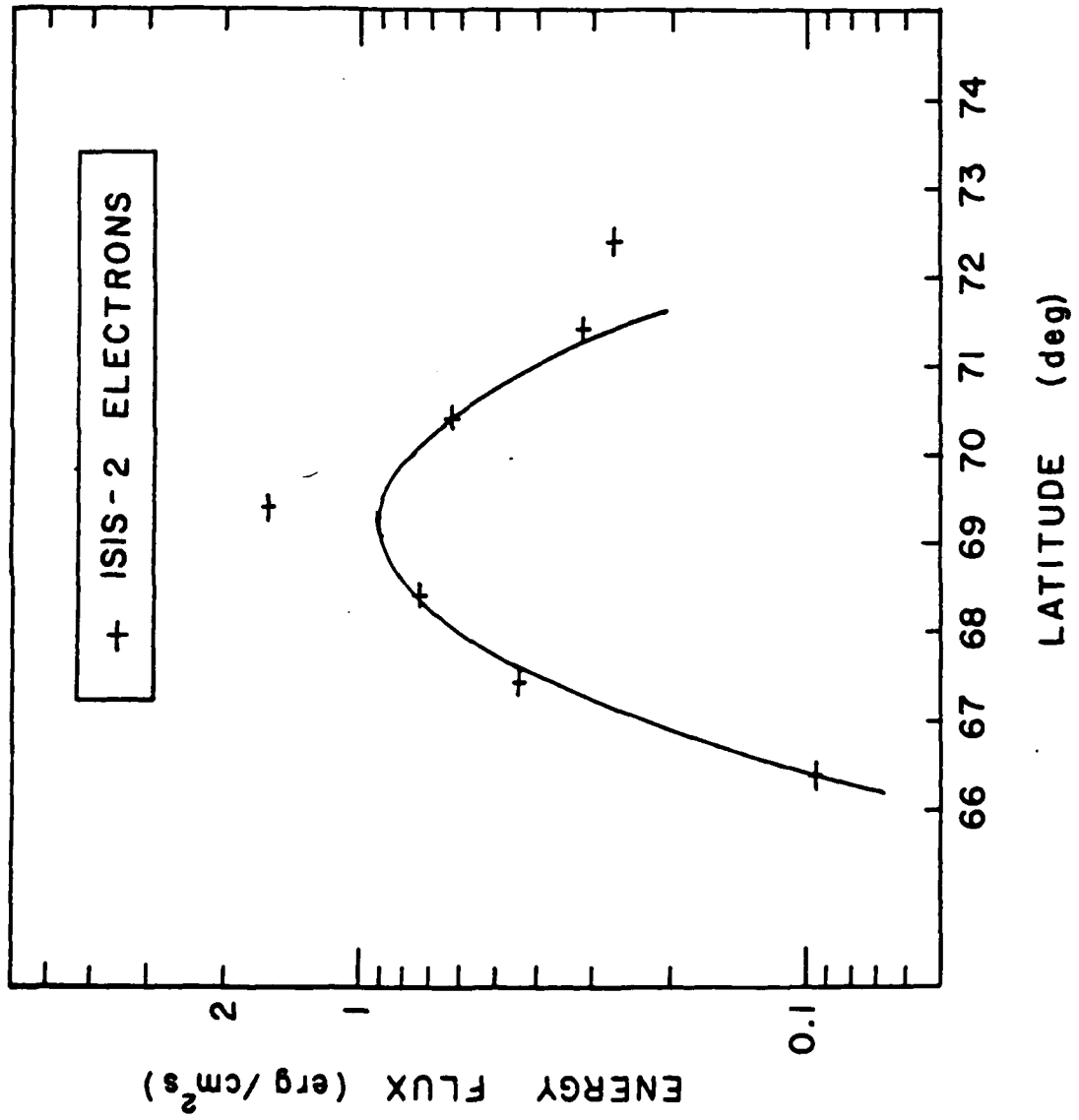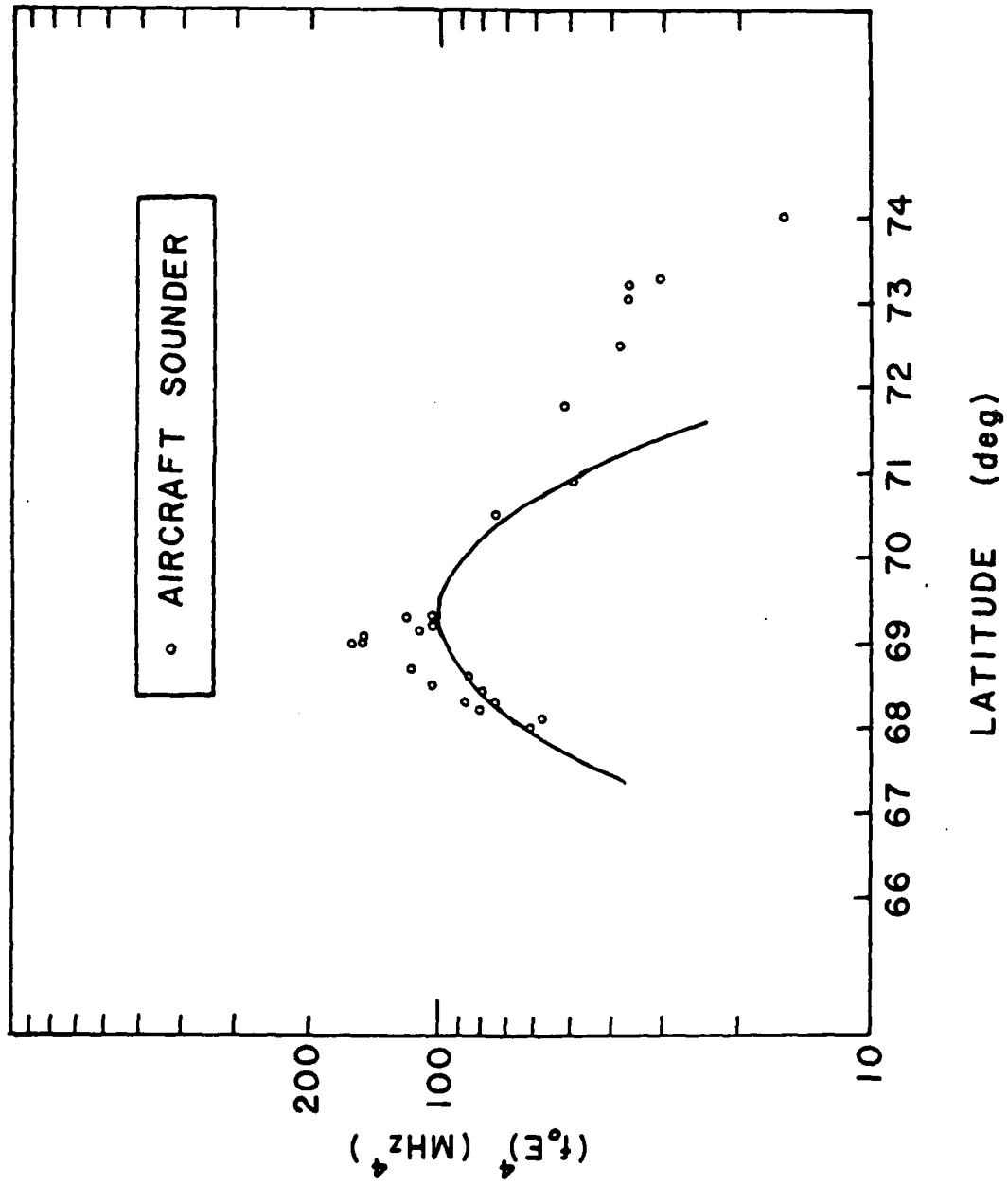
LATITUDE (deg)

— ISIS-2 ELECTRONS
· AIRCRAFT SOUNDER
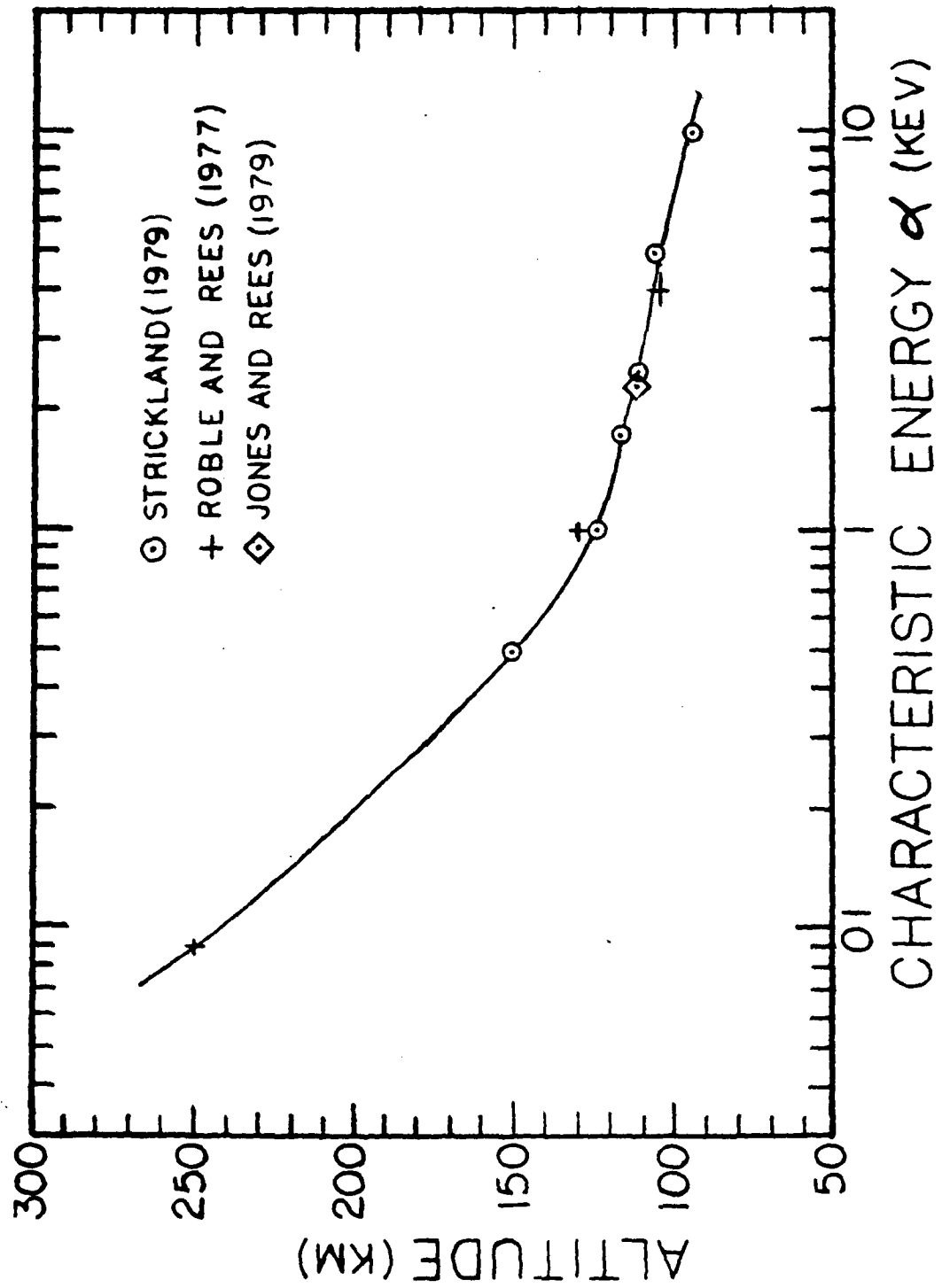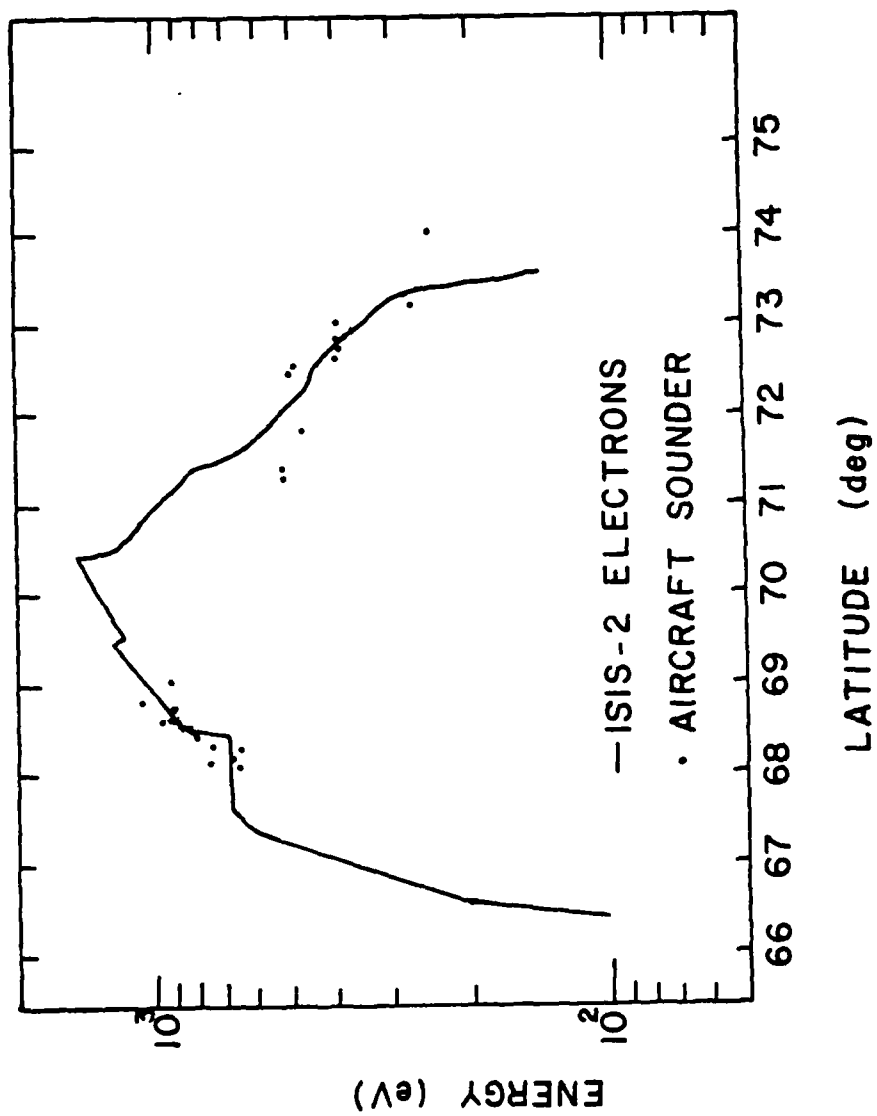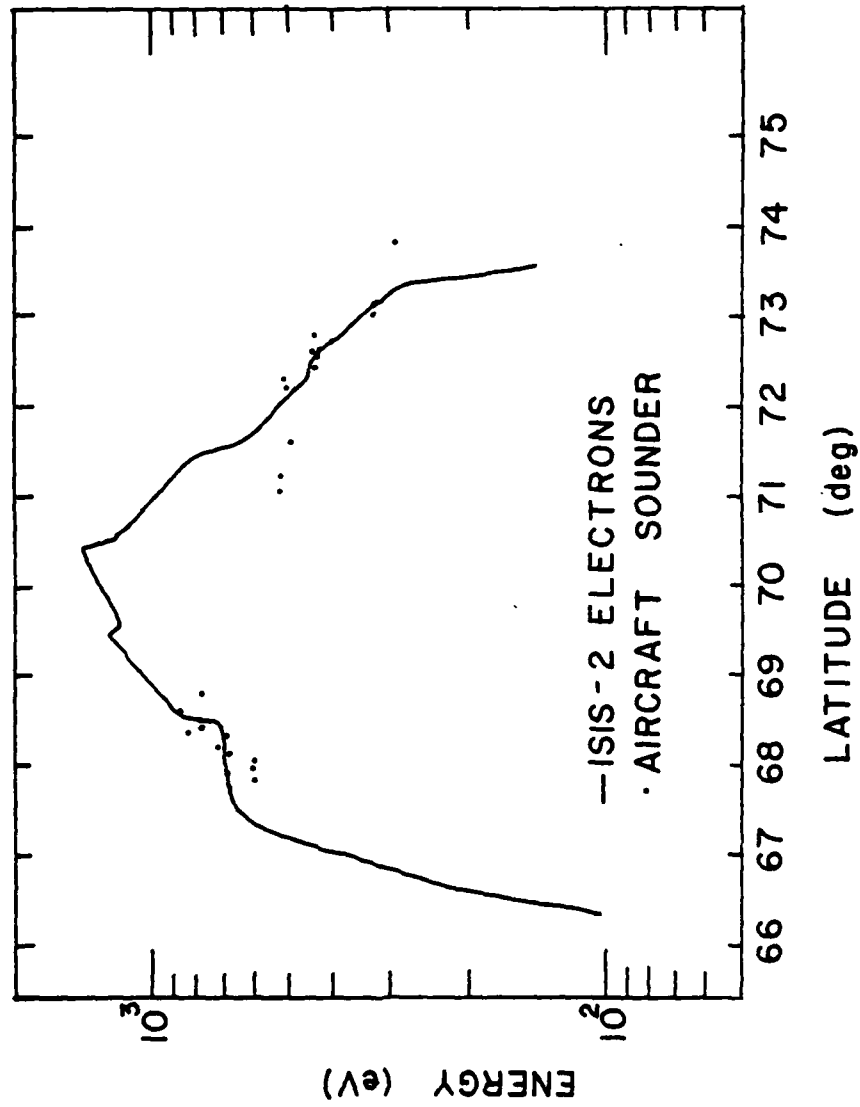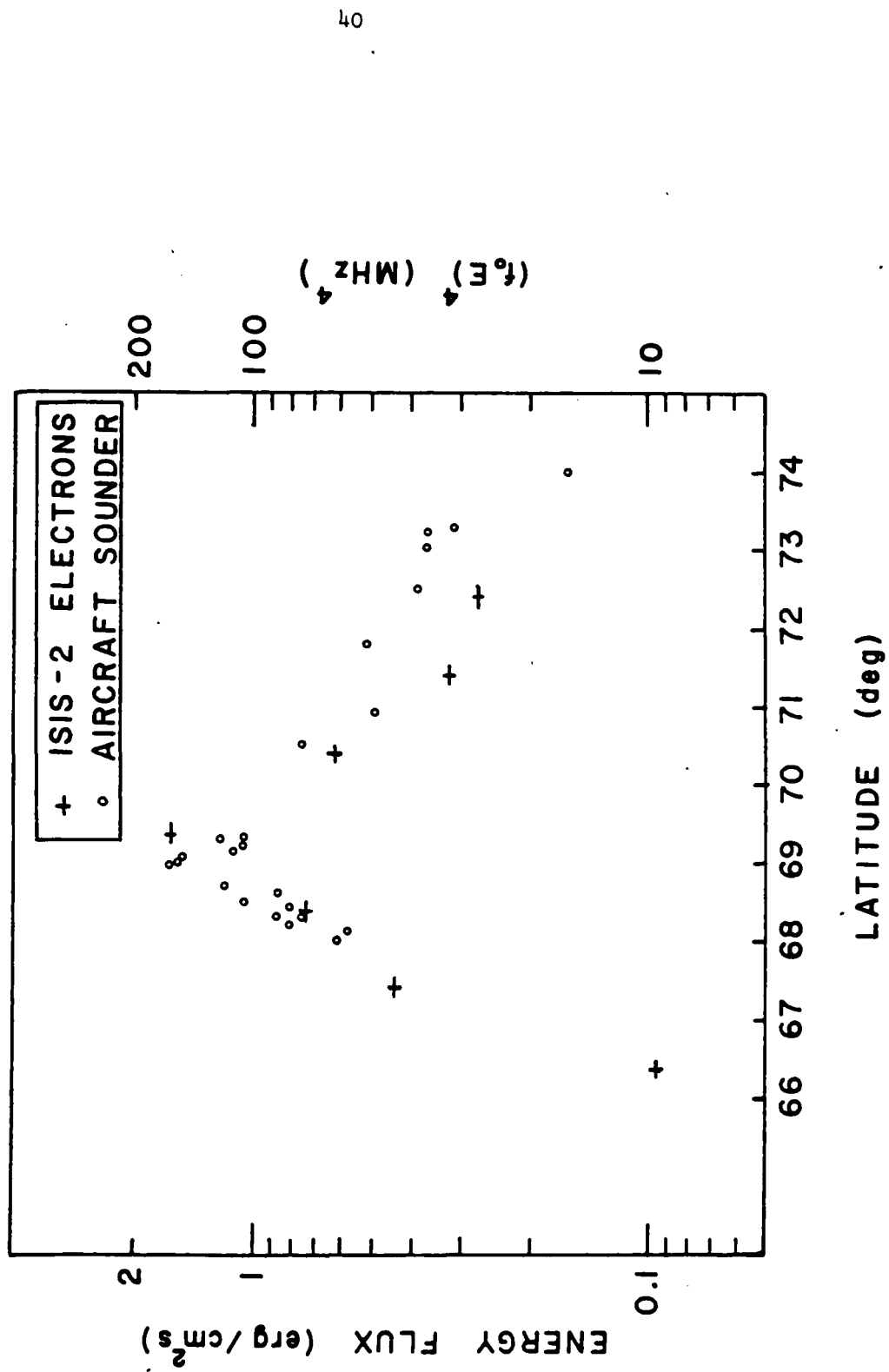
Figure 10

Figure 11

Figure 12

Figure 13
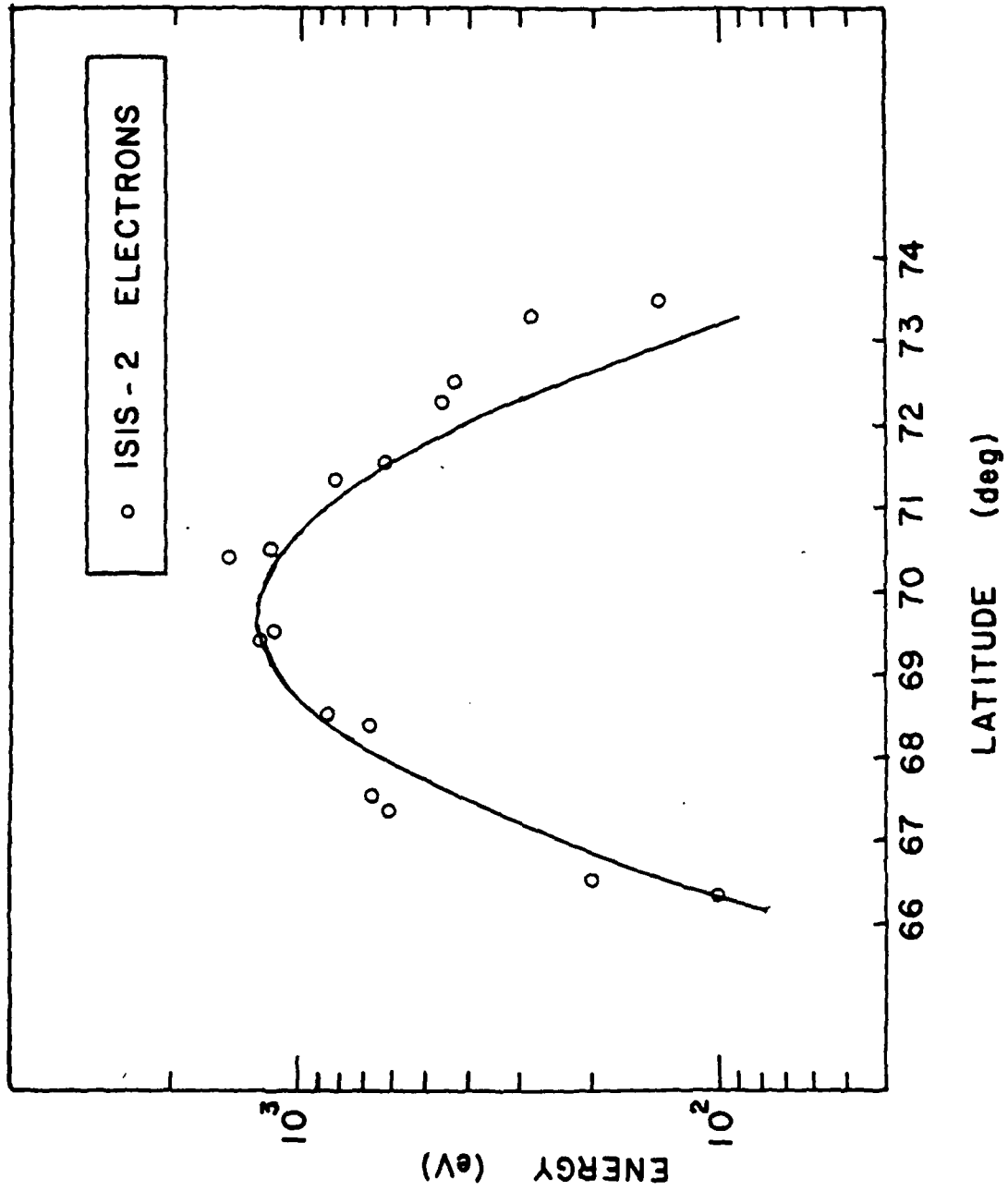
Figure 14
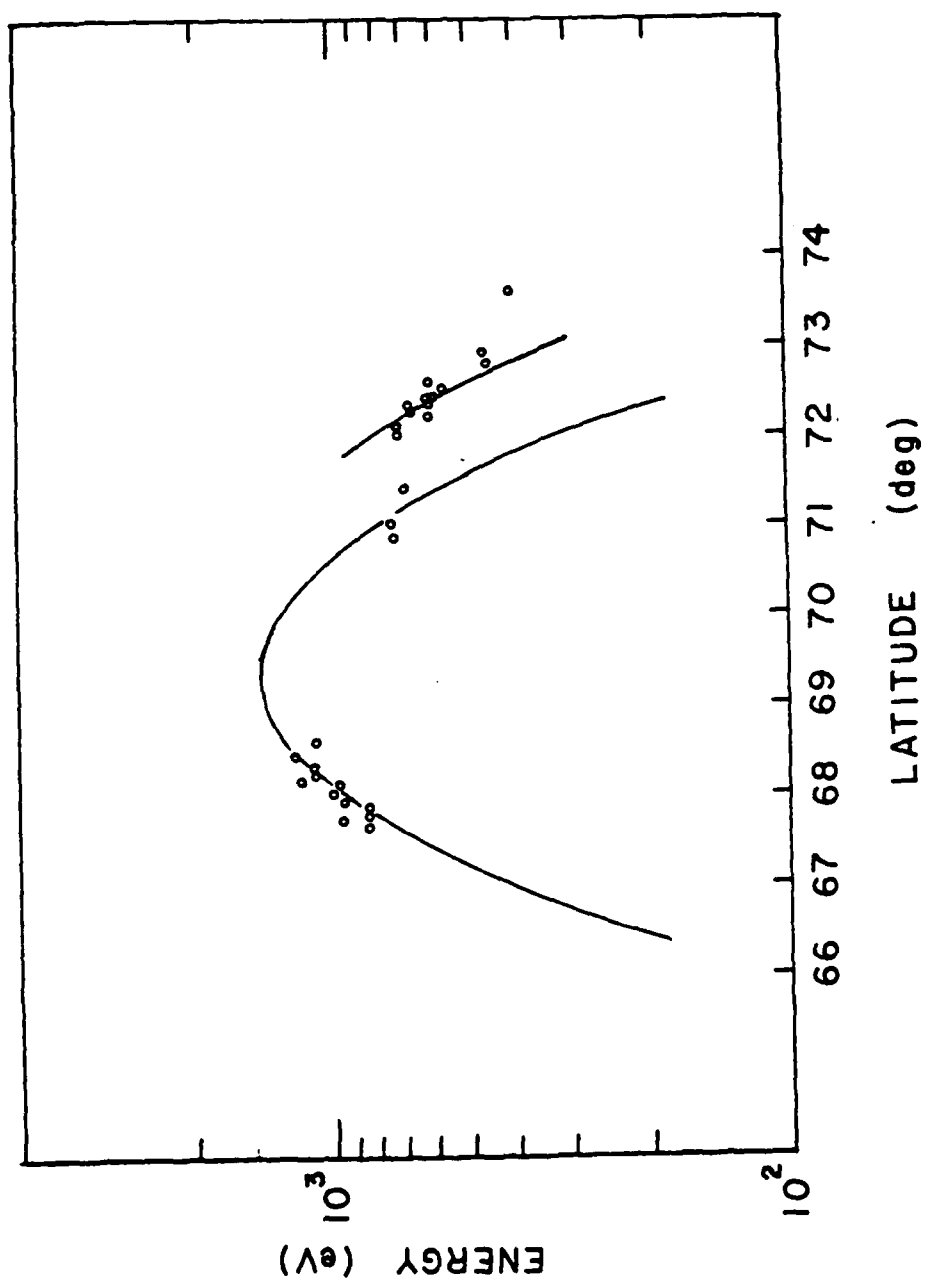
Figure 15
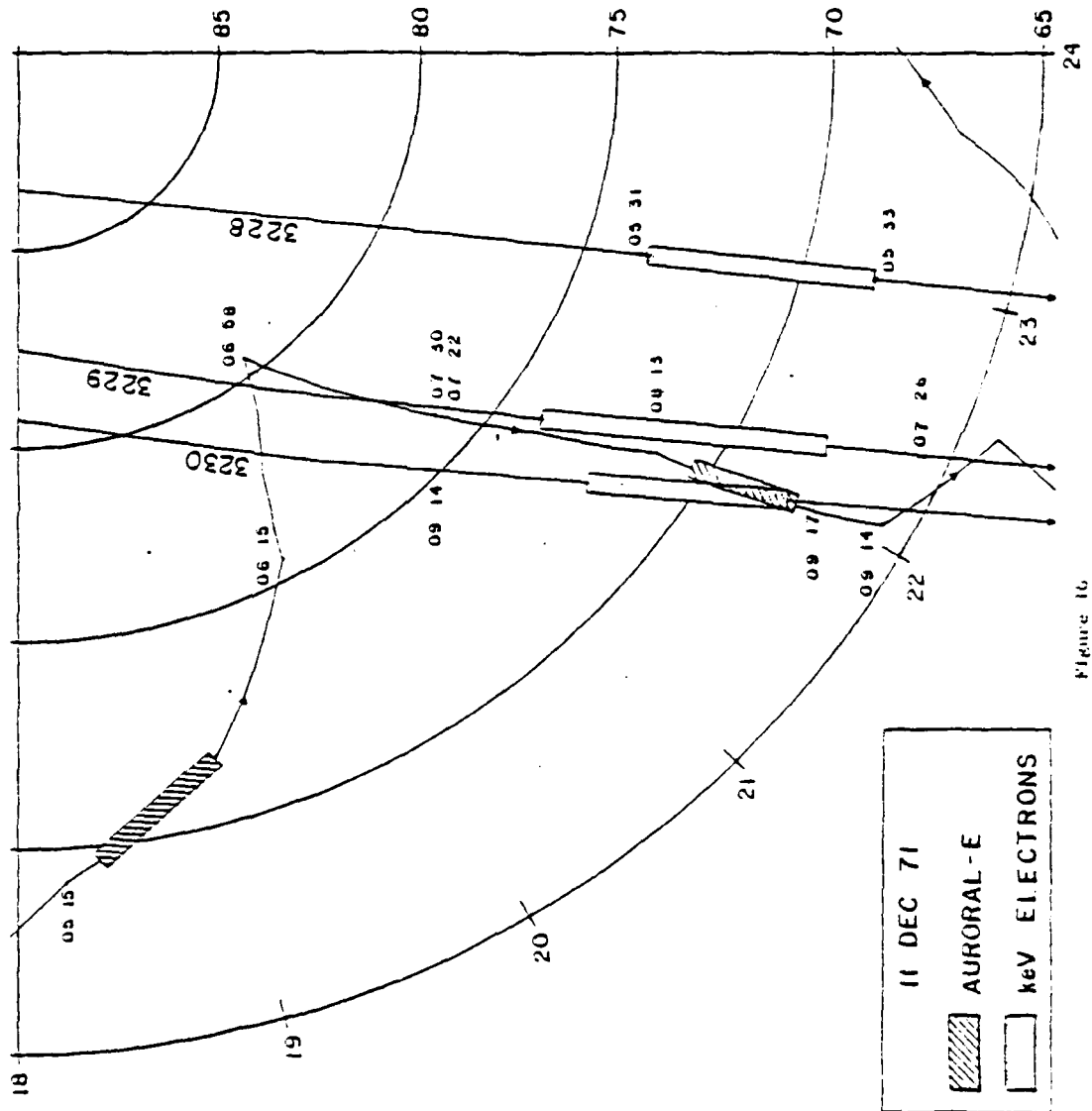
Figure 16

11 DEC 71

AURORAL-E

keV ELECTRONS

Figure 17

Uniform Field Boundaries
$E = 1 \, kV/R_E$

12 keV

4.5 keV

0.75 keV

0 keV

0000

0600

1800

1200

ATS-5

−2

−4

−6

−8

−10
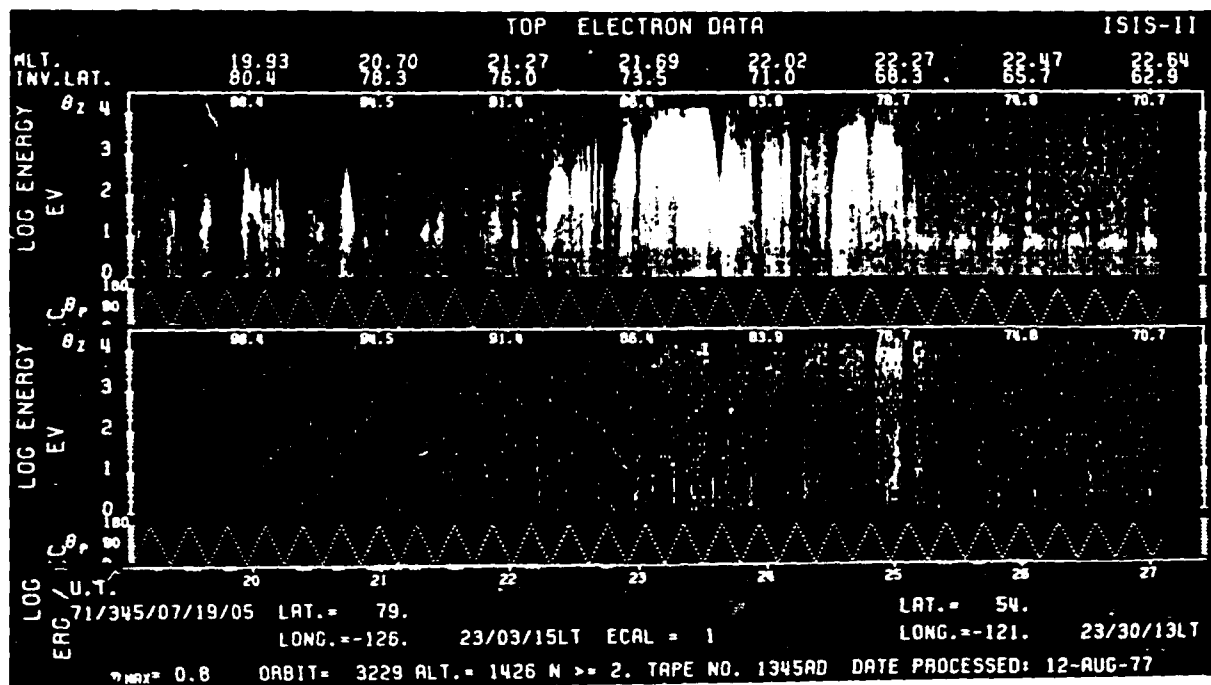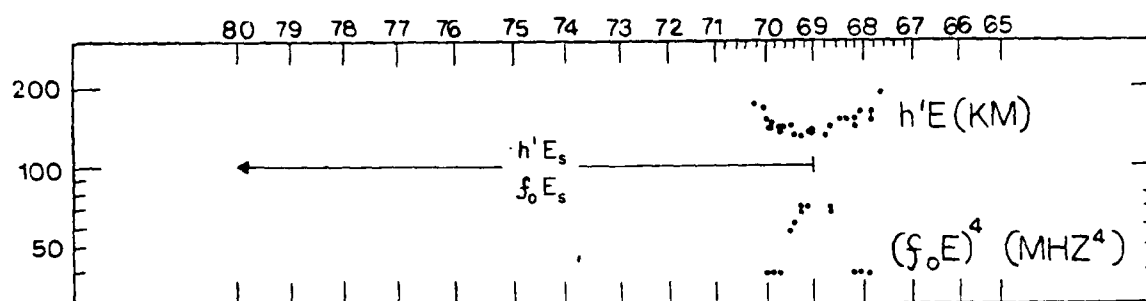
Figure 18

Figure 19

Figure 20

APPENDIX A

THE ISIS-2 SOFT PARTICLE SPECTROMETER

The ISIS-2 soft particle spectrometer package, similar to that in ISIS-1 (Heikkila et al., 1970), is a divergent plate electrostatic analyzer. The package actually contains two separate deflection systems, one positioned atop 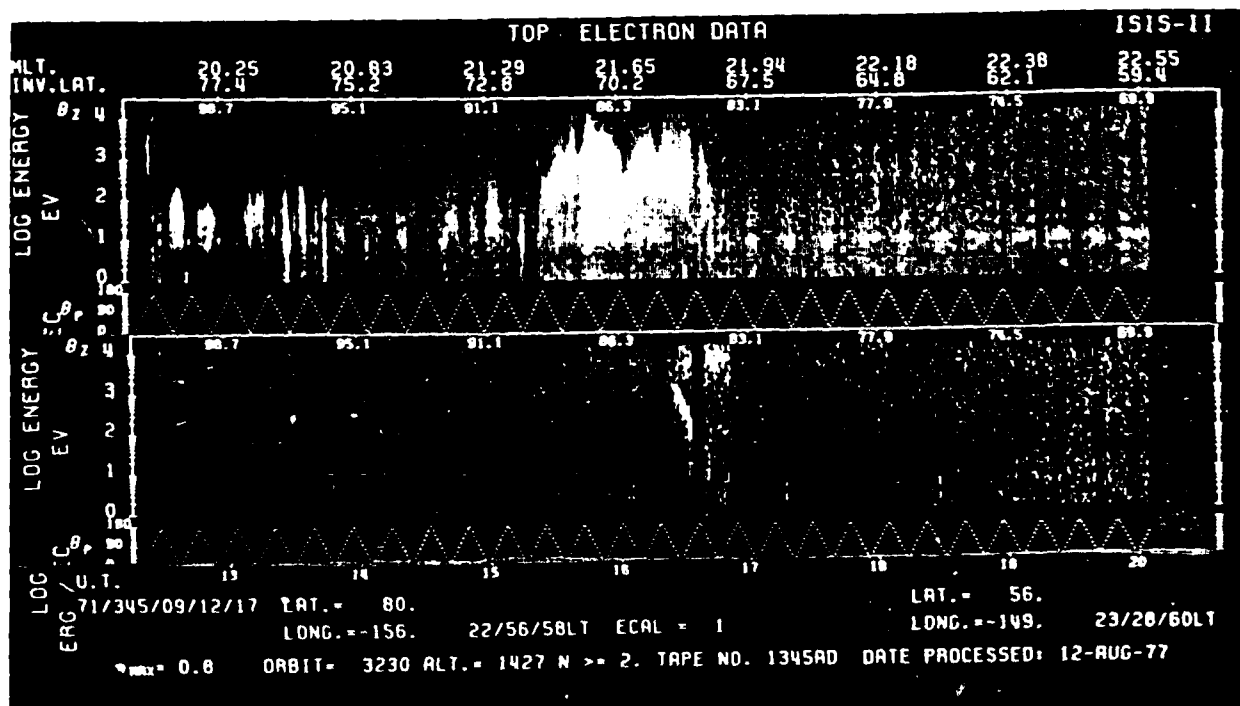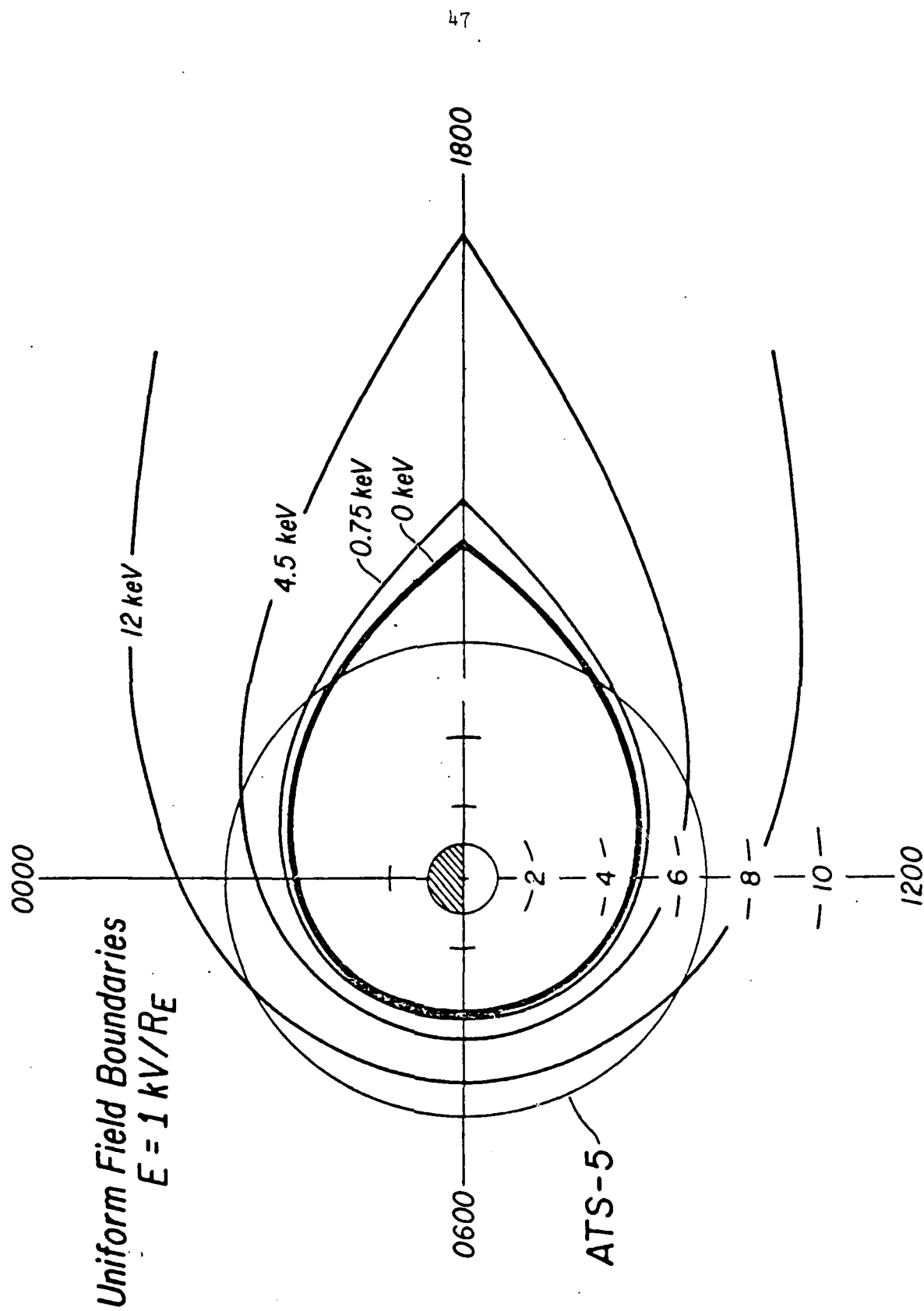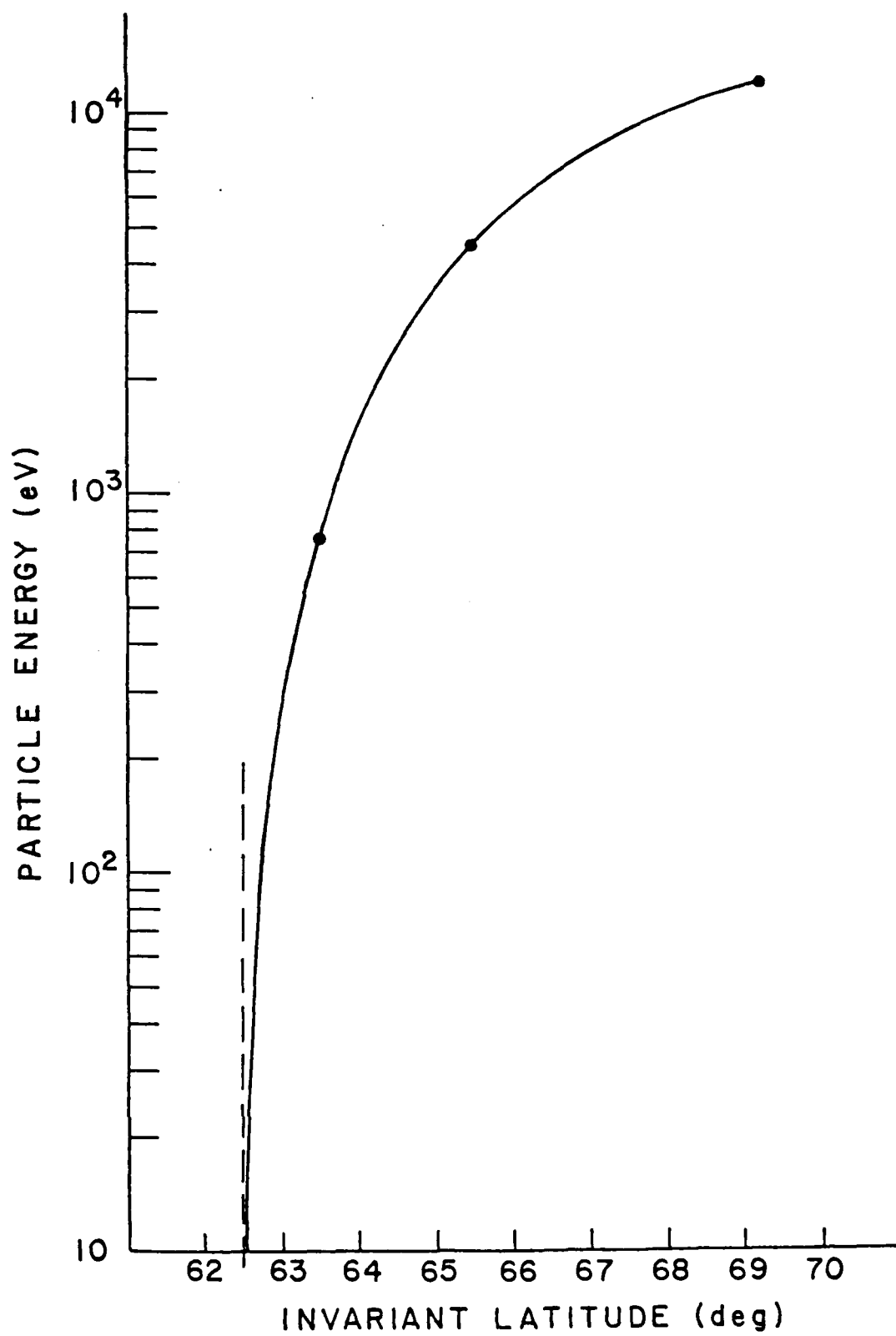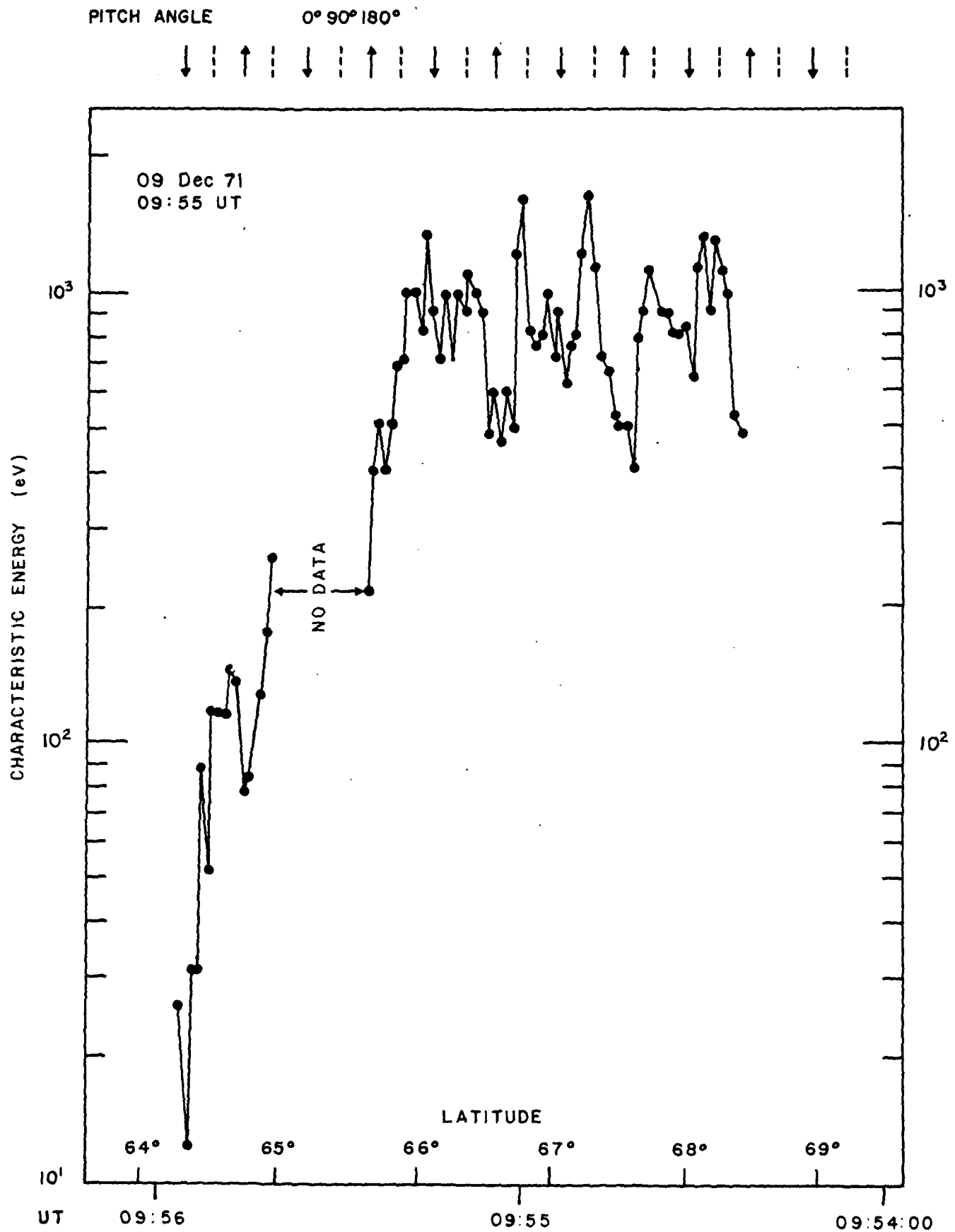the other, each with its own collimation system, deflection plates, and particle sensors (discrete dynode multipliers). In the normal mode of operation electrons are analyzed by the top system, protons by the bottom system. The top (electron) analyzer has an energy resolution ($\Delta E/E$) of 0.247, a geometric factor of 3.95×10^{-4} cm^2 sr. The bottom (proton) analyzer has an energy resolution of 0.247 and a geometric factor of 1.27×10^{-3} cm^2 sr. The deflection systems have identical rectangular collimators with the result that the effective angular responses are very nearly the same. The angular half angles are 5° in the satellite equatorial plane and 15° in the meridional plane.

A spectrum is measured by sampling the detector outputs as the potential difference between the deflection plates decays exponentially through values which correspond to energies of 13.2 keV and 5.5 eV for the electron analyzer and 14.7 and 6.2 eV for the proton detector. The accumulation time for each data sample is 0.0111s and a complete spectral measurement is made simultaneously for electrons and protons each second. The center energies of the samples, the sample bandwidths and the measured detection efficiencies of the multipliers (Bunting et al., 1972) are listed in Table A.1.

TABLE A.1. ISIS 2 SOFT PARTICLE SPECTROMETER CHARACTERISTICS

	ELECTRON DETECTOR				PROTON DETECTOR		
Sample	Center Energy $E_0(eV)$	Bandwidth ΔE (ev)	Efficiency η	Sample	Center Energy $E_0(eV)$	Bandwidth ΔE (ev)	Efficiency η
1	13150	3248	.230	1	14675	5210	.8
2	12620	3117	.235	2	14084	5000	.8
3	9805	2422	.270	3	10942	3884	.8
4	7919	1956	.295	4	8837	3137	.8
5	6395	1580	.320	5	7137	2534	.8
6	5165	1276	.350	6	5764	2046	.8
7	4171	1030	.375	7	4655	1653	.8
8	3369	832	.400	8	3759	1334	.8
9	2721	672	.430	9	3036	1078	.8
10	2197	543	.460	10	2452	870	.8
11	1774	438	.495	11	1980	703	.8
12	1433	354	.535	12	1599	568	.8
13	1157	286	.575	13	1292	459	.8
14	935	231	.620	14	1043	370	.8
15	755	186	.665	15	842	299	.8
16	610	151	.705	16	680	241	.8
17	492	122	.735	17	549	195	.8
18	398	98.3	.760	18	444	158	.8
19	321	79.3	.778	19	358	127	.8
20	259	64.0	.790	20	289	103	.8
21	209	51.6	.800	21	234	83.1	.8
22	169	41.7	.800	22	189	67.1	.8
23	137	33.8	.800	23	152	54.	.8
24	110	27.2	.790	24	123	43.7	.8
25	89.1	22.0	.782	25	99.4	35.3	.8
26	72.0	17.8	.772	26	80.3	28.5	.8
27	58.1	14.4	.764	27	64.9	23.0	.8
28	46.9	11.6	.755	28	52.4	18.6	.8
29	37.9	9.36	.748	29	42.3	15.0	.8
30	30.6	7.56	.738	30	34.2	12.1	.8
31	24.7	6.10	.730	31	27.6	9.8	.8
32	20.0	4.94	.721	32	22.3	7.92	.8
33	16.1	3.98	.715	33	18.0	6.39	.8
34	13.0	3.21	.710	34	14.5	5.15	.8
35	10.5	2.59	.705	35	11.7	4.15	.8
36	8.5	2.10	.700	36	9.5	3.37	.8
37	6.9	1.70	.700	37	7.7	2.73	.8
38	5.5	1.36	.700	38	6.2	2.20	.8

APPENDIX B

THE SUMMING FUNCTION $f(\theta_i, \theta_z)$

The amount of energy per unit area per unit time crossing an area normal to the magnetic field direction from within a cone of half angle θ is given by

$$Q = \int Q(\theta) \cos \theta \, d\Omega \tag{B.1}$$

where $Q(\theta)$ represents the pitch angle distribution of energy and $d\Omega$ is the differential increment of solid angle. If θ is defined as the polar angle, the increment of solid angle may be written as $2\pi \sin \theta \, d\theta$, which results in

$$Q = \pi \int Q(\theta) \sin 2\theta \, d\theta \tag{B.2}$$

For a detector on a rotating satellite successive measurements are made over finite intervals of pitch angle so that the integral of equation (B.2) must be replaced by a finite sum

$$Q = \pi C \sum_i Q_i(\theta_i, \theta_z) \sin 2\theta_i \, \Delta\theta_i \tag{B.3}$$

where θ_i is the pitch angle at which the i th measurement is made. The angle θ_z is the angle between the satellite spin axis (the z axis) and the local magnetic field direction. (See Figure B.1) The factor C (3.2 for ISIS-2) adjusts for the fact that the half width of the angular response ($\Delta\psi_e = 5.0^{\circ}$) in the satellite equatorial plane is 0.313 times the angular interval ($\Delta\psi = 16.0^{\circ}$) scanned between successive measurements.

Two points about equation (B.3) should be mentioned. First, the finite sum is taken only over pitch angles actually scanned by the satellite, and since the pitch angle scan is only over the range $90^{\circ} \pm \theta_z$, pitch angles near 0° will in general be excluded. This will result in a slight underestimate of the integral flux.

The second point regards the angular interval $\Delta\theta_i$ in pitch angle space. Figure (B.2) shows the position of the center of the detector aperture for rotational angular intervals $\Delta\psi$ between 0° and 90° as the detector makes a scan. Latitude lines drawn through each mark along BP intersect the arc of the great circle PR. It is clear that the projections onto PR of the equal intervals of the arc BP decrease in length as the detector approaches $\psi = 90^\circ$ (or approaches a pitch angle of $90^\circ - \theta_z$). Thus as the detector rotates, successive measurements become more closely spaced in pitch angle as the minimum value $90^\circ - \theta_z$ is approached. This effect is compensated for by multiplying each measurement by $\cos\beta$ (see Figure B.2). $\cos\beta$ may be found by noting that the triangle ABC is a right spherical triangle. The following relation applies:

$$\cos\beta = \sqrt{\sin^2\theta_z - \cos^2\theta}/\sin\theta$$

Thus the angular interval $\Delta\theta$ of pitch angle space may be related to the angular interval $\Delta\psi_e$ actually scanned by the detector as

$$\Delta\theta = \sqrt{\frac{\sin^2\theta_z - \cos^2\theta}{\sin\theta}}\ \Delta\psi_e \tag{B.4}$$

Combining equations (B.3) and (B.4) the general expression for the finite sum becomes

$$Q = 2\pi C \sum_i Q_i(\theta_i,\ \theta_z) \cos\theta_i \sqrt{\sin^2\theta_z - \cos^2\theta_i}\ \Delta\psi_{ei} \tag{B.5}$$

ISIS-2 makes two pitch angle scans per spin cycle. If both scans are used in the sum, the expression for the integrated energy becomes

$$Q = (0.876) \sum_i Q_i(\theta_i,\ \theta_z) \cos\theta_i \sqrt{\sin^2\theta_z - \cos^2\theta_i} \tag{B.6}$$

or

$$Q = \sum_i Q_i(\theta_i, \theta_z) \, f(\theta_i, \theta_z) \qquad\qquad \text{B.7}$$

If only one scan is used, the constant is doubled and becomes 1.754.

Figure B.3 shows a family of curves of $f(\theta_i, \theta_z)$ from equation B.7 plotted

vs. pitch angle θ_i for 10° increments of θ_z from 20° to 80°. The expression

represents the sum over any range of pitch angles scanned by the detector.

To determine the amount of energy lost to the ionosphere the sum is carried

out only for pitch angles within the loss cone. At the ISIS-2 altitude

of 1400 km this is 49.5° at auroral latitudes for the passes of 09 December

71.

APPENDIX B FIGURE CAPTIONS AND FIGURES

Fig. B.1: Orientation of the ISIS-2 satellite with respect to the local

magnetic field line B. As the satellite rotates, the detector

scans pitch angles of $90^\circ - \theta_z$ to $90^\circ + \theta_z$.

Fig. B.2: Cut-away view on the unit sphere showing the relationship between

the satellite spin axis Ω, the detector normal N and the local

magnetic field direction z. The figure is the basis for equation

B.4 which relates increments of the rotation angle $\Delta\psi$, along arc

BP, to increments of pitch angle $\Delta\theta$ along arc PR.

Fig. B.3: The summing function $f(\theta, \theta_z)$ plotted against pitch angle θ for

values of θ_z in 10° increments from 20° to 80°.

ISIS-2

SPIN VECTOR

DETECTOR
NORMAL

θ

θ_z

B

Figure B.1

$\Psi = BOA$
$\Theta = QOA$
$\Theta_Z = ZO\Omega$

$\Delta\Theta = \Delta\Psi COS(\beta)$
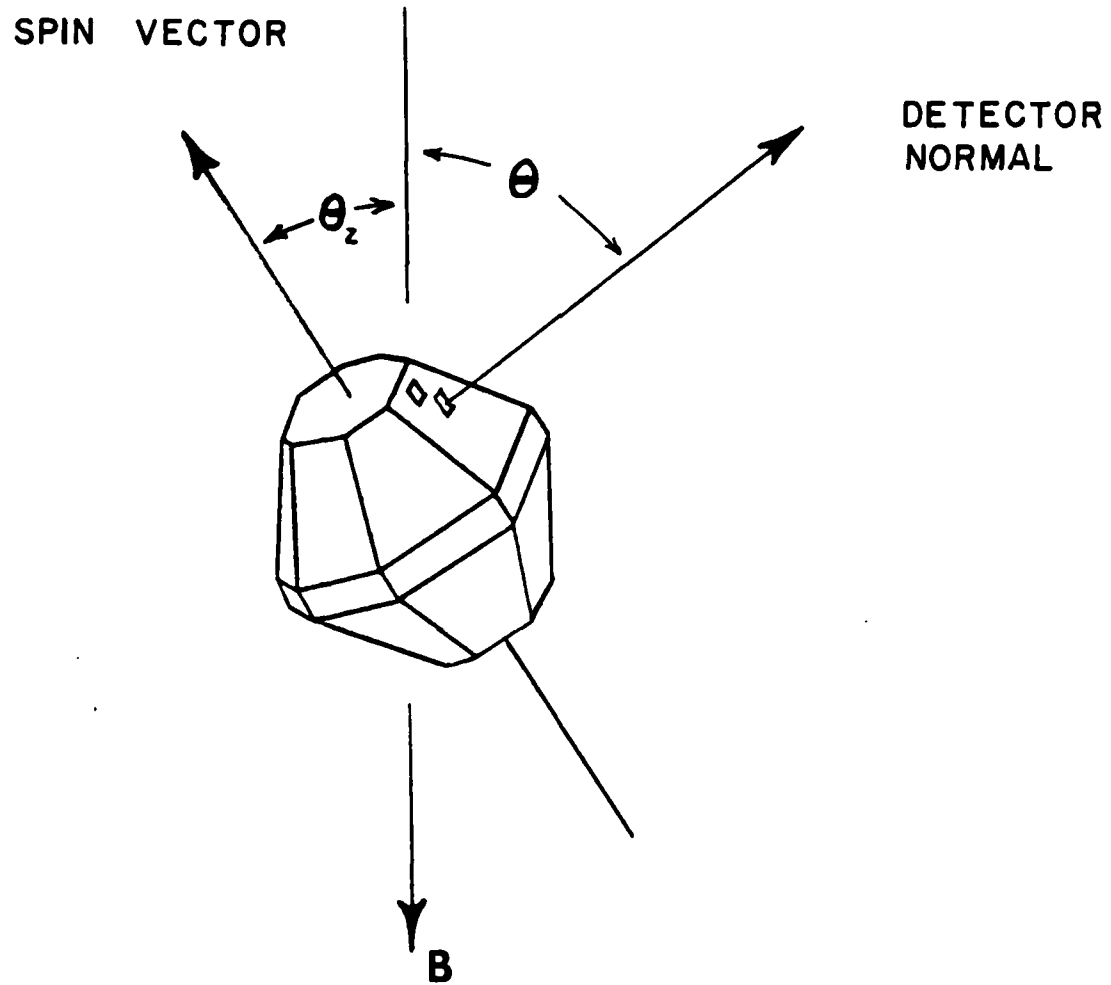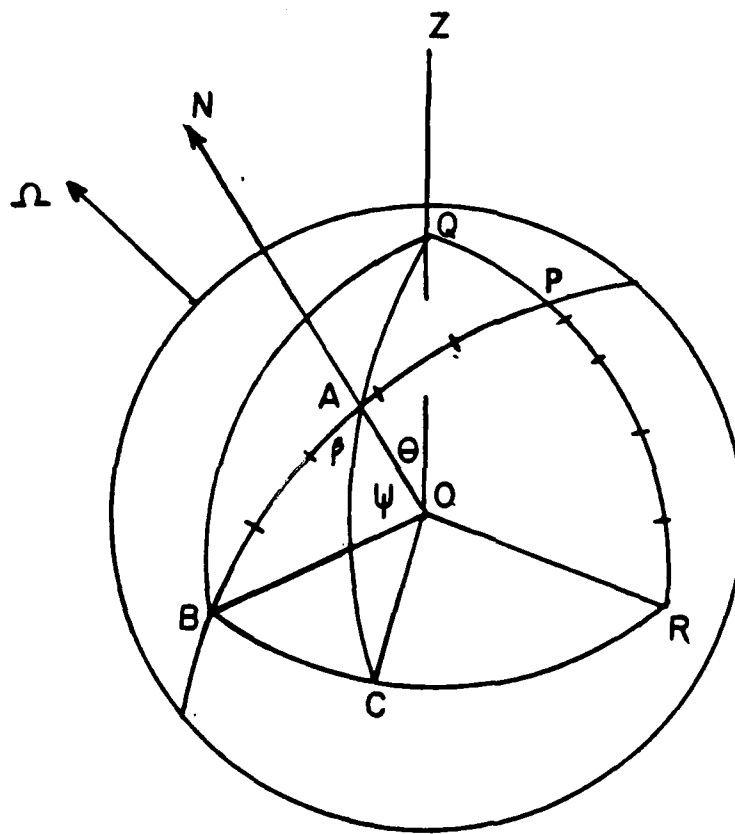
Figure B.2

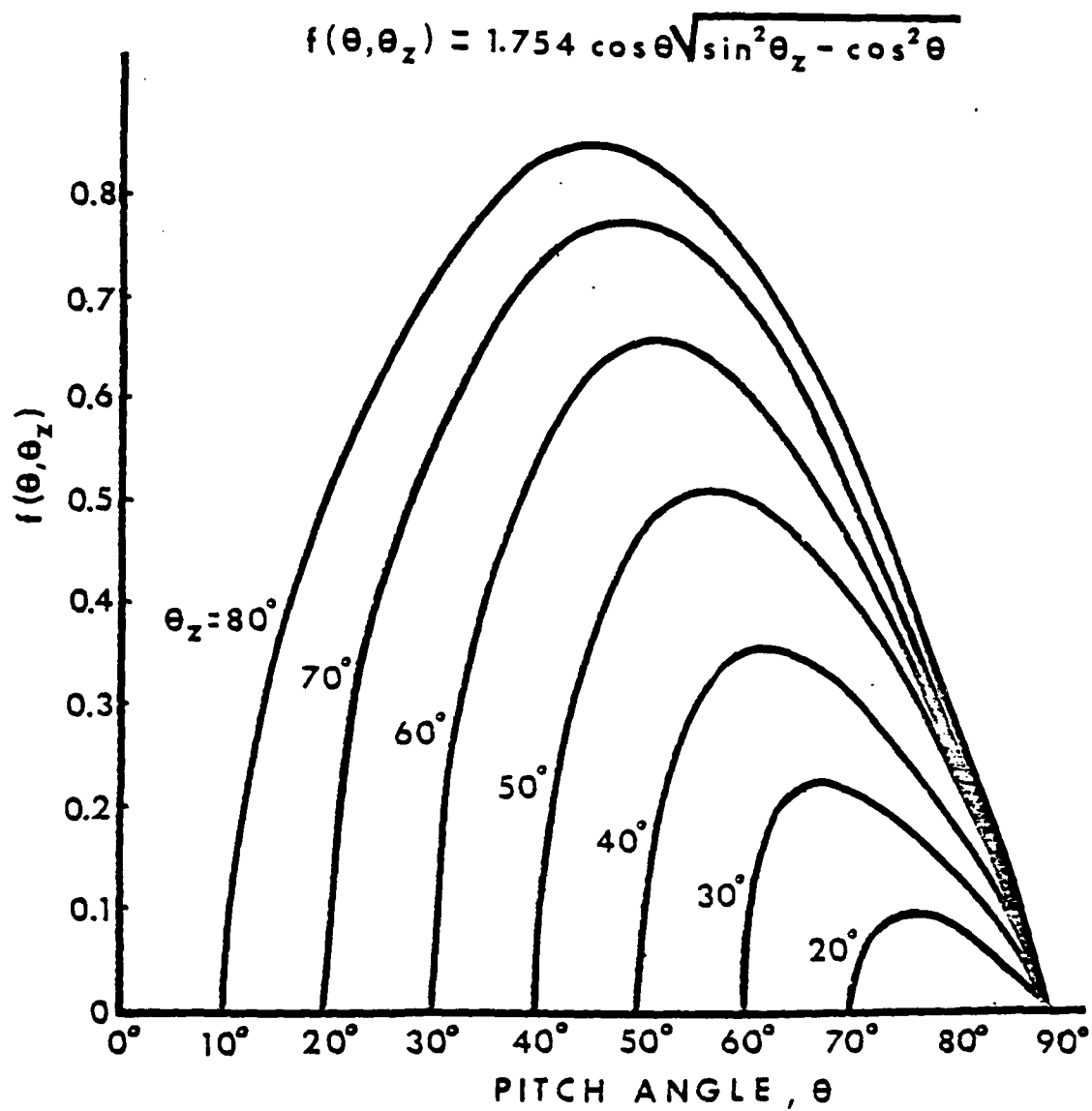$$f(\theta,\theta_z) = 1.754 \cos\theta \sqrt{\sin^2\theta_z - \cos^2\theta}$$

Figure 3.3

13. REFERENCES

Bresprozvanaya, A. S., and T. I. Shchuka, Possible nature of the auroral-E Layer, Geomagnetism and Aeronomy, 17, 22, 1977.

Bunting, W. D., Jr., J. Tarstrup, and W. J. Heikkila, Detection efficiency of electron multipliers for low-energy electrons, J. Appl. Phys., 43. 1972.

Deehr, Charles Sterling, J. David Winningham, Fumihiko Yasuhara, and Syun-Ichi Akasofu, Simultaneous observations of discrete and diffuse auroras by the ISIS-2 satellite and airborne instruments, J. Geophys. Res., 81, 5527, 1976.

Eather, R. H., and F. Jacka, Auroral hydrogen emission, Aust. J. Phys., 19, 1966.

Eather, R. H., and K. M. Burrows, Excitation and ionization by auroral protons, Aust. J. Phys., 19, 309, 1966.

Frank, L. A., Relationship of the plasma sheet, ring current, trapping boundary, and plasmapause near the magnetic equator and local midnight, J. Geophys. Res., 76, 2265, 1971.

Heikkila, W. J., J. B. Smith, J. Tarstrup, and J. D. Winningham, The soft particle spectrometer in the ISIS-1 satellite, Rev. Sci. Instruments, 41, 1393, 1970.

Hulquist, Bengt, Rocket and satellite observations of energetic particle precipitation in relation to optical aurora, Ann. Geophys., 30, 223, 1974.

Jones, Vallance A., Aurora, D. Reidel, Dordrecht, Netherlands, 1974.

Jones, R. A., and M. H. Rees, Time dependent studies of the aurora. 1, Ion density and composition, Planet. Space Sci., 21, 537, 1973.

Kaye, S. M., and M. G. Kivelson, Time dependent convection electric fields and plasma injection, J. Geophys. Rev., 84, 4183, 1979.

Kivelson, J. G., S. M. Kaye, and D. J. Southwood, The physics of plasma injection events, submitted to Rev. Geophys. and Space Phys., 1979.

Lui, A. T. Y., D. Vankatesan, C. D. Anger, S.-I. Akasofu, W. J. Heikkila, J. D. Winningham, and J. R. Burrows, Simultaneous observations of particle precipitations and auroral emissions by the ISIS-2 satellite in the 19-24 MLT sector, J. Geophys. Rev., 82, 2210, 1977.

Mahlem, B., The sporadic-E auroral zone, Geofys. Publikasjoner Norsk Videnskajss - Akad. Oslo, 23, 1, 1962.

Meng, C.-I., Simultaneous observations of low-energy electron precipitation and optical auroral arcs in the evening sector by the DMSP-32 satellite, J. Geophys. Res., 81, 2771, 1976.

Montalbett, R., and D. J. McEwen, Hydrogen emissions and sporadic E-layer behavior, J. Phys. Soc. Japan, 17, 212, 1962.

Omholt, A., The auroral-E layer ionization and the auroral luminosity, J. Atmosph. Terr. Phys., 7, 73, 1955.

Pike, C. P., J. A. Whalen, and J. Buchau, A 12-hour case study of auroral phenomena in the midnight sector: F-layer and 6300 Å measurements, J. Geophys. Res., 82, 3547, 1977.

Rees, M. H., Note on the penetration of energetic electrons into the earth's atmosphere, Planet. Space Sci., 12, 722, 1964.

Roble, R. G., and M. H. Rees, Time-dependent studies of the aurora: effects of particle precipitation on the dynamic morphology of ionospheric and atmospheric properties, Planet. Space Sci., 25, 991, 1977.

Strickland, D. J., Determination of E-region electron density profiles for the continuous aurora, Quarterly Status Report, 6, Prepared for Department of the Air Force, 1979.

Vasyliunas, V. M., A survey of low-energy electrons in the evening sector of the magnetosphere with 060 1 and 060 3, J. Geophys. Res., 73, 2839, 1968.

Weber, E. J., J. A. Whalen, R. A. Wagner, and J. Buchau, A 12-hour case study of auroral phenomena in the midnight sector: electrojet and precipitating particle characteristics, J. Geophys. Res., 82, 3557, 1977.

Whalen, James A., Jurgen Bachau, and Rosemarie A. Wagner, Airborne ionospheric and optical measurements of noontime aurora, J. Atmosph. Terr. Phys., 33, 661, 1971.

Whalen, J. A., R. A. Wagner, and J. Buchau, A 12-hour case study of auroral phenomena in the midnight sector: oval, polar cap, and continuous auroras, J. Geophys. Res., 82, 3529, 1977.

Whalen, J. A., and J. R. Sharber, Integration over the loss cone of electrons in the continuous (diffuse) aurora: Gaussian latitudinal profile, presented at Spring 1979 Meeting of the A.G.U., abstract: EØS, 60, 355, 1979.

Winningham, J. D., A case study of the aurora, high-latitude ionosphere, and particle precipitation during near-steady state conditions, J. Geophys. Res., 83, 5717, 1978.

Winningham, J. D., F. Yasuhara, S.-I. Akasofu, and W. J. Heikkila, The latitudinal morphology of 10-eV to 10-keV electron fluxes during magnetically quiet and disturbed times in the 2100-0300 MLT sector, J. Geophys. Res., 72, 3148, 1975.

14. PUBLICATIONS

Presented Papers

Two papers reporting preliminary results of this study were presented at the Spring 1979 Meeting of the American Geophysical Union. Abstracts follow:

(1) SM 93: E⊕S, 60, 1979, p. 355; INTEGRATION OVER THE LOSS CONE OF ELECTRONS IN THE CONTINUOUS (DIFFUSE) AURORA: THE MAXWELLIAN CHARACTER OF THE SPECTRUM; James R. Sharber (Department of Physics and Space Sciences, Florida Institute of Technology, Melbourne, FL 32901); James A. Whalen (Ionospheric Dynamics Branch, Air Force Geophysics Laboratory, Hanscom AFB, MA 01731).

Measurements from the ISIS-2 Soft Particle Spectrometer show that, except near the peak of the latitudinal profile of the continuous aurora, the electron total energy in the range of a few hundred eV to $\simeq$ 13 keV is not isotropic over the loss cone. In fact, the total energy measured at pitch angles between 0° and $\simeq 20^{\circ}$ is less by as much as a factor of two than that measured near the edge of the loss cone. This anisotropy accounts for the observation that the electron spectrum is well represented by a Maxwellian distribution at pitch angles nearer the edge of the loss cone, but is rather poorly represented by the Maxwellian at the low pitch angles. The anisotropy must be carefully considered in determining the amount of energy deposited in the upper atmosphere during continuous auroras. It is found that when spectra measured at pitch angles within the loss cone are appropriately integrated, the result is a Maxwellian spectrum. It's total energy, determined from its characteristic energy and peak flux, accurately represents the total energy deposited in the E region.

(2) SM94: E⊕S, 60, 1979, p. 355; INTEGRATION OVER THE LOSS CONE OF ELEC-

TRONS IN THE CONTINUOUS (DIFFUSE) AURORA: GAUSSIAN LATITUDINAL PROFILE;

J. A. Whalen (Ionospheric Dynamics Br., Air Force Geophysics Laboratory,

Hanscom AFB, MA 01731); J. R. Sharber (Department of Physics and Space

Sciences, Florida Institute of Technology, Melbourne, FL 32901).

In the continuous (diffuse) aurora near midnight and in the absence

of discrete aurora, electrons are found to have Maxwellian kinetic

energy spectra when integrated over the loss cone. Under these condi-

tions the Maxwellian characteristic energy has a latitudinal profile

which is well represented by a Gaussian distribution of about 3° (full

width at half maximum) in invariant latitude. The precipitated energy

flux in such cases has approximately this same Gaussian latitudinal

distribution and thus a precipitated electron number flux which is rela-

tively latitude independent. Photometric measurements also detect a

Gaussian latitudinal profile in the precipitated energy flux in the

quiet time continuous aurora. Ionospheric soundings from aircraft are

consistent with the approximate latitude independence of the number

flux for this aurora.

Preparation for Publication

In addition three publications are currently being undertaken. Papers

will likely be submitted to the Journal of Geophysical Research or Planetary

and Space Physics. Tentative titles and descriptions follow:

(1) Relation Between the Incident Electron Spectrum of the Diffuse Aurora

and Properties of Auroral-E Ionization with J. A. Whalen.

This paper is based on sections 2-5 of the current report and will (a) describe the particle spectrum of the diffuse aurora, (b) present the results of integration of the angular distribution of electrons over the loss cone, and (c) show how the characteristic and total energies of the incident spectrum relate to the virtual height and critical frequency respectively of the auroral-E region.

(2) Colocation of Auroral-E Ionization and the Earthward Extension of the Central Plasma Sheet with J. A. Whalen and J. D. Winningham.

This paper will be taken from chapters 6 and 7 of this report. It will have one purpose: to demonstrate that the auroral-E layer is observed over the same range of latitudes as the extension to auroral latitudes of the central part of the plasma sheet.

15. ACKNOWLEDGMENTS